ACTA TECNOLOGÍA

electronic journal
ISSN 2453-675X
Volume 10
Issue 2
2024

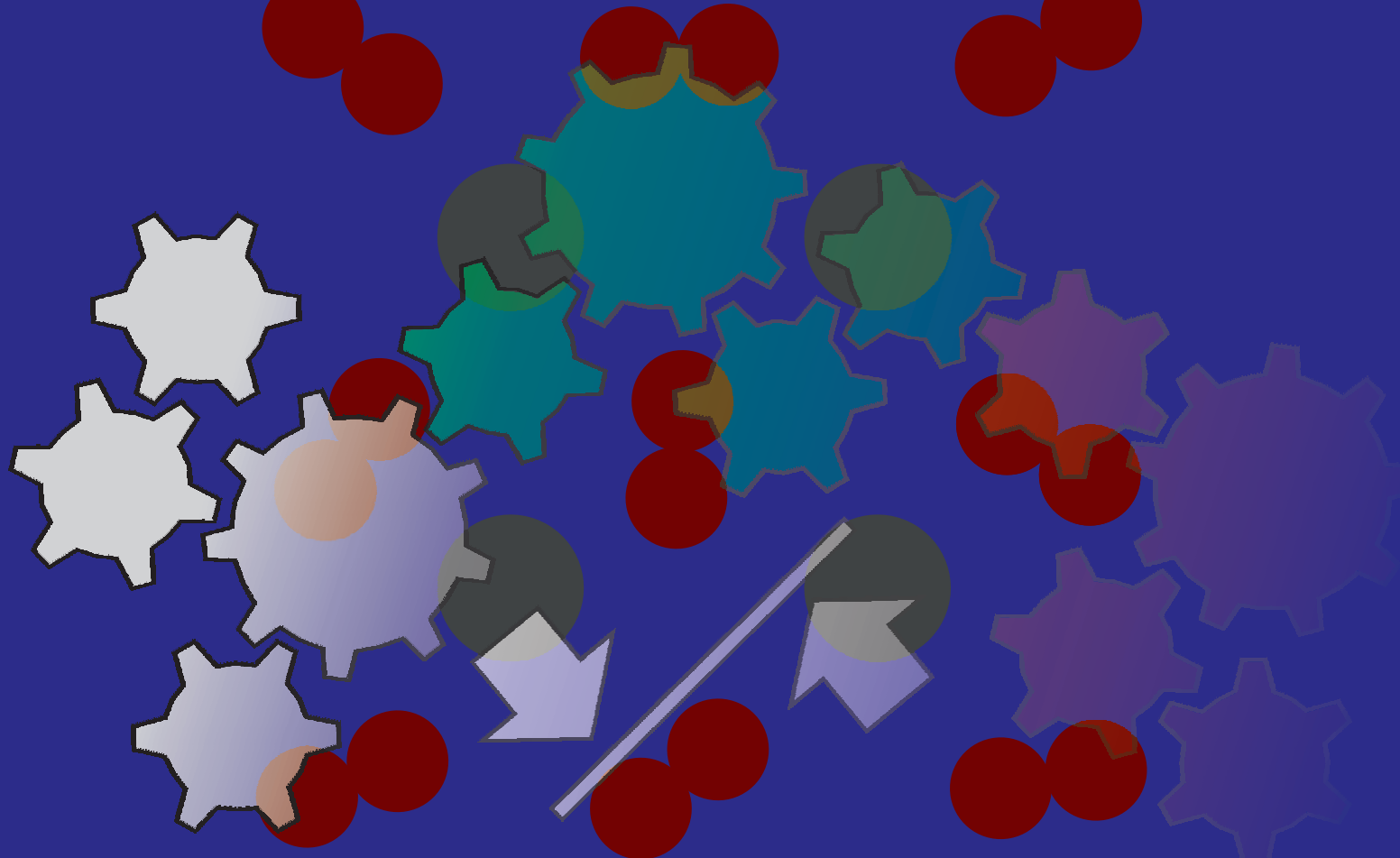

International Scientific Journal about Technologies

CONTENTS
(JUNE 2024)

Acta Tecnología - International Scientific Journal about Technologies
Volume: 10 2024 Issue: 2 Pages: 45-49 ISSN 2453-675X

https://doi.org/10.22306/atec.v10i2.198 Received: 02 Apr. 2024; Revised: 27 June 2024; Accepted: 29 June 2024

The use of alginate in the cultivation of mesenchymal cells in biomedical engineering

Darina Bacenkova
Faculty of Mechanical Engineering, Technical University of Kosice, Department of Biomedical Engineering and Measurement, Letná 1/9, 040 01 Košice, Slovak Republic, EU,
darina.bacenkova@tuke.sk (corresponding author)
Jana Demeterova
Faculty of Mechanical Engineering, Technical University of Kosice, Department of Biomedical Engineering and Measurement, Letná 1/9, 040 01 Košice, Slovak Republic, EU,
jana.demeterova@tuke.sk
Erik Dosedla
Department of Gynecology and Obstetrics, Faculty of Medicine, Pavol Jozef Šafarik Univerzity Hospital AGEL Košice-Šaca, Pavol Jozef Šafarik University in Košice, 04015 Košice-Šaca, Slovak Republic, EU,
erik.dosedla@nke.agel.sk
Petra Gasparova
Department of Gynecology and Obstetrics, Faculty of Medicine, Pavol Jozef Šafarik Univerzity Hospital AGEL Košice-Šaca, Pavol Jozef Šafarik University in Košice, 04015 Košice-Šaca, Slovak Republic, EU,
petra.gasparova01@nke.agel.sk
Marianna Trebunova
Faculty of Mechanical Engineering, Technical University of Kosice, Department of Biomedical Engineering and Measurement, Letná 1/9, 040 01 Košice, Slovak Republic, EU,
marianna.trebunova@tuke.sk

Keywords: alginate, stem cells, biomedical engineering.
Abstract: Stem cells are a specialized type of cells in a human or animal organism that have the ability to self-renew and differentiate into various types of cells in the body. They have great potential in medical research and therapies as they can be used to treat a variety of diseases, regenerate tissues and develop new therapeutic approaches. In the article, we describe the cultivation of stem cells with alginate, which is used in 3D cultivation. The biopolymer alginate is preferred in biomedical applications due to its excellent properties. Polysaccharide alginate is isolated from marine, brown algae and bacterial cultures of species, *Azotobacter* and *Pseudomonas* species. Alginate is soluble in water, which allows easy processing and application in the form of various hydrogels or matrices. We present the preparation of alginate gel in the form of beads in combination with multiplied stem cells under in vitro conditions. At the same time, we observed how a natural polymer, specifically alginate, which is used for cultivation, behaves towards cells and how it affects their proliferation and differentiation.

1 Introduction

A characteristic feature of stem cells is the undifferentiated state of cells with the ability to differentiate into any cell type of the human organism and at the same time the ability to self-renew. They are found in embryos, but also in the cells of adult individuals. The division of stem cells is not limited, which allows them to replace other cells in the body again. During the division of each stem cell, there is a possibility that it differentiates into a somatic cell with a specific function, for example, into muscle or nerve cells, or it can remain in the form of a stem cell [1]. Thanks to their properties, stem cells offer enormous potential in the field of regenerative medicine and the therapy of various disorders.

Polysaccharide alginate is isolated from marine, brown algae and bacterial cultures of species, *Azotobacter* species and *Pseudomonas* species. In the case of bacteria, alginate forms a protective capsule, supports the formation of a biofilm and helps with adherence and colonization. Due to its ability to form hydrogels, alginate is widely used as a stabilizing and thickening agent and emulsifier. Alginate is, after cellulose, the most widespread biopolymer available worldwide [2].

1.1 Alginate

The extraction of alginate from natural, plant sources involves several processes. In the first phase, a mineral acid acts, which changes the salts of alginic acid (called alginates) contained in algae into free alginic acid. This step is followed by a process of neutralization with sodium bicarbonate or sodium hydroxide, whereby soluble sodium alginate is formed. The purification of this soluble alginate is carried out with either calcium chloride or mineral acid and the product is insoluble fibers of calcium alginate and

a gel form of alginic acid. The mentioned substances are subsequently mixed with sodium bicarbonate to form sodium alginate.

Sodium alginate is a substance that is the most desired form of alginate salt prepared industrially. In addition to the mentioned form, calcium alginate, potassium alginate and ammonium alginate are industrially prepared [4].

Calcium alginate is isolated by a similar procedure. Potassium alginate and ammonium alginate are made by adding the appropriate hydroxide, usually potassium carbonate or ammonium hydroxide, to the alginic acid gel [5].

1.2 Structure of alginate

Alginates are composed of 1,4-linked β-D-mannuronic acid (M) and 1,4 α-L guluronic acid (G) residues that form blocks of repeating G residues, repeating M residues, and alternating G residues and M (Figure 1). The composition and sequence of G and M residues depends on the type of natural sources used for alginate extraction. It has been proposed that only the carboxylate groups of G residues form conductive bonds with divalent cations such as Ca^{2+}, Mg^{2+} to form hydrogels. Alginates with high G content form tough hydrogels hydrogels, while alginates with high M content form softer elastic hydrogels. The approximate molecular weight of alginate is ranges from 32,000 to 400,000 g/mol. As the molecular weight of alginate increases, its viscosity increases during the preparation of the gel. Although alginate is usually considered a biocompatible, non-toxic and non-immunogenic material, there are opinions that alginate with a high content of the mannuronic (M) component may be more immunogenic compared to alginate with a high content of the guluronic (G) component [2].

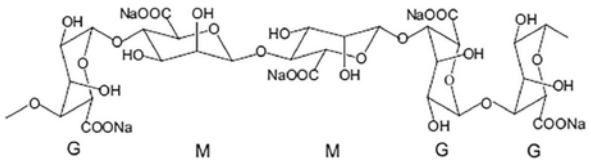

Figure 1 Chemical structure of alginate composed of 1,4-linked residues of β-d-mannuronic acid M and 1,4 α-l-guluronic acid G [2]

1.3 Properties of alginate

The biopolymer alginate is preferred in biomedical applications due to its excellent properties. Its main properties include the ability to form gel structures in the presence of divalent cations, especially calcium (Ca^{2+}).

In addition, alginate is known for its low toxicity to human cells and organisms, making it a safe material for use in biomedicine. Alginate is soluble in water, which allows easy processing and application in the form of various hydrogels or matrices. Its chemical composition contains acid and hydroxyl groups, which allows various chemical modifications, such as cross-linking with divalent cations or modification of properties for specific applications in biomedicine. Combined with these properties, alginate is a useful material for various applications in biomedicine, such as drug carriers, biological matrices for tissue engineering, or the basis for specific types of bioactive materials [3].

To improve the physical characteristics of alginate, other substances are often added, resulting in alginate composites. Other substances are often added to improve the physical properties of alginate, resulting in alginate composites. Natural polymers, collagen, chitosan and gelatin, as well as synthetic polymers, polylactides and polypyrrole, and inorganic compounds, tetraethylorthosilicate (TEOS) and hydroxyapatite (HA) are most often used as additives for alginate composites. The mixture was also tested with other types of materials such as ceramics, bioglass, inorganic nanoparticles and inorganic carbon materials.

Multiple alginate composites are currently used for clinical application in the form of gel wound treatment. For the use of alginate composites in various biomedical applications, they are molded into fibers, beads, hydrogels or 3D-printed materials for the specific requirements of each biomedical application [6].

1.4 The role of alginate in biomedical engineering

Alginate is characterized by its unique properties advantageous in biomedical applications, but it also has certain disadvantages. Mutual interactions between monovalent cations and alginate blocks cause instability of the gels. Unbound polymer blocks are not naturally degraded by enzymatic processes in humans. Although the resulting gel material dissolves in the organism, the alginate molecules themselves are difficult to completely eliminate, because the average molecular weight of commercially available alginates exceeds the renal clearance limit of the kidneys. However, alginate as a biopolymer of natural origin, which exhibits many unique properties and is more suitable for tissue engineering, has several significant disadvantages [7].

However, alginate is characteristically non-degradable for mammals, because there is no enzyme (alginase) that could break down the polymer chain of alginate. Partially oxidized alginate can degrade in water, which makes alginate a promising material for drug and cell delivery in various applications. Sodium periodate is used to oxidize alginate, which can break the carbon-carbon bonds in the *cis*-diol group of uronate. This process changes the conformational structure of alginate to an open chain and promotes the decomposition of the main structure of alginate [3].

Another disadvantage of alginate is its weaker ability to allow cell adhesion, resulting in less cell interaction and adhesion with both the 3D and 2D surroundings.

However, alginate hydrogels can support minimal protein adsorption due to its hydrophilic property. Therefore, alginate hydrogels alone are unable to support

cell migration and adhesion but can be refined on a 2D surface or inside a 3D hydrogel, where they form multicellular bundles. To make alginate a suitable material for tissue engineering applications, it is necessary to increase its degradation rate through chemical modifications such as gamma irradiation or partial oxidation and by adding cell-bound materials such as RGD-containing proteins or peptides. These materials can be conjugated with alginate to promote cell adhesion. The chemical structure of RGD is shown in Figure 2 [3].

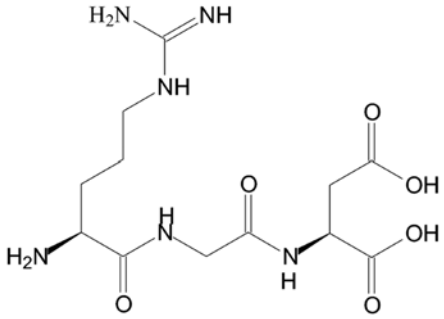

Figure 2 Chemical structure of RGD [3]

2 Methodology

2.1 Isolation of stem cells

The process of isolating stem cells from the amnion-chorion membrane begins with obtaining these fetal membranes after a planned section at the Gynecology and Obstetrics Clinic of the Agel Košice-Šaca Hospital from healthy pregnant women with their prior consent. This material is then transferred to the sterile laboratory conditions of KBIaM, where it is further processed in a laminar box to maintain its sterility.

2.2 3D cell culture in alginate

The process of 3D culture of stem cells in alginate starts with trypsinization of chorionic mesenchymal stem cells (CMSCs) when they are at the stage of approximately 80% formation of the monolayer of adherent cell layer. At the beginning, the cultivation bottle T75 is prepared. Subsequently, we added 4.0 ml of 0.25% trypsin EDTA to each bottle, which helps to disrupt intercellular junctions and release adhered cells from the surface. Trypsinization was observed under a microscope to assess its effectiveness and was allowed to act for another 3 minutes. After the completion of trypsinization and inactivation of trypsin by adding a 20% solution of bovine serum in DMEM, we prepared the cells for 3D cultivation. First, we prepared a 1% solution of alginate in physiological solution, which we sterilized by filtration. To create gelling spheroids, the so-called "alginate beads", we used a solution of 0.1 M $CaCl_2$. CMSCs cells were resuspended in a 1% alginate solution at a concentration of 1 million cells/ml and, using a 2 ml pipette, we applied the solution drop by drop into the $CaCl_2$ solution. In contact with $CaCl_2$, rapid polymerization of alginate occured, while the cells were trapped inside the spheroids. $CaCl_2$ solution was aspirated from the polymerized spheroids and they were washed with the medium without additives. To ensure optimal conditions for the cells, we placed the spheroids in a complex culture medium (e.g. alpha MEM / DMEM with 10% FBS and 1% antibiotics/antimycotics) (Figure 3) and incubated at 37 °C and in an atmosphere with 5% CO_2. We regularly changed the culture medium every 2-3 days, which ensured a constant supply of nutrients and removal of metabolic waste. We monitored the overall condition and development of the cell culture in a 3D environment regularly under a microscope to monitor the morphology and health of the cells.

Figure 3 Change of the culture medium

3 Results

Isolation and cultivation of stem cells: After the successful isolation of stem cells, their cultivation followed. This process was aimed at monitoring cell proliferiation growth in a controlled environment. During the first 2-3 days after isolation, the culture medium was regularly checked and changed when necessary, which helped to eliminate non-adherent erythrocytes and other unwanted cells. This care allowed the cells to adapt to the new environment. The culture medium was systematically changed twice a week, which ensured optimal conditions for the growth and development of the culture. This approach not only promoted cell growth, but also minimized the risk of contamination. After two weeks of intensive care and monitoring, we were able to see the formation of a monolayer culture of adhered cells. This culture was characterized by its purity, as it did not contain any hematopoietic cells, indicating a high efficiency of the isolation and culture process. The stem cells showed a healthy morphology and a consistent proliferation rate, indicating their good adaptation to the culture environment (Figure 4). Thanks to regular checks and maintenance of

the medium, we have recorded minimal to no contamination, which additionally confirms the effectiveness of our sterilization and cultivation techniques.

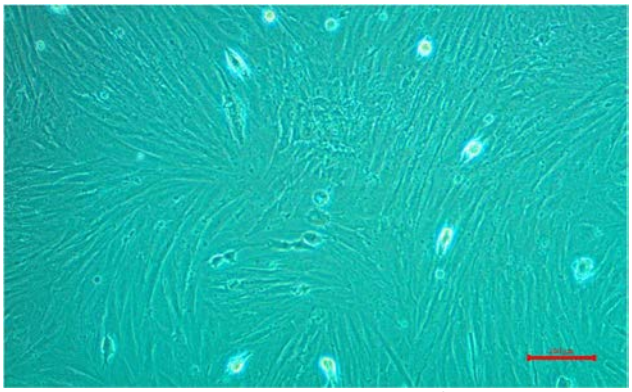

Figure 4 Stem cells: day 6 passage (magnification under the microscope 10x)

3D cell culture in alginate: During our 14-day 3D cultivation of stem cells in alginate, we regularly changed the culture medium every 2-3 days, thereby ensuring optimal conditions for cell growth and development. Systematic monitoring of the cell culture under the microscope allowed us to observe their proliferation, morphology and overall health in a three-dimensional environment. The results of our observation showed that the cells in the alginate matrix maintained their natural morphology and showed significant proliferation. These results confirmed that the 3D culture environment provides conditions that effectively mimic the natural cellular environment, which is critical for studies related to cell interaction and differentiation (Figure 5).

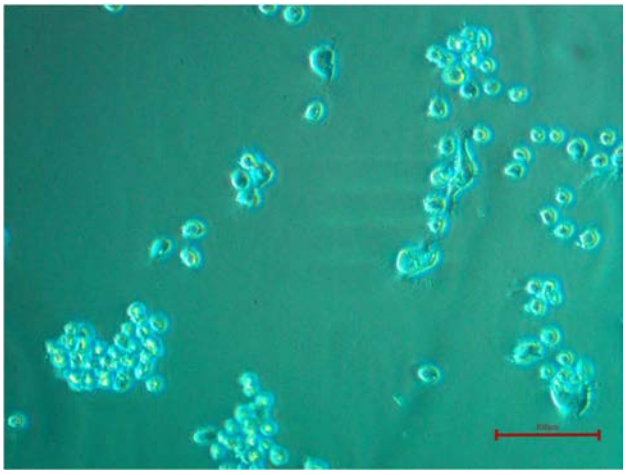

Figure 5 Stem cells: passage day 6 in alginate (magnification under the microscope 20x)

4 Conclusion

This work dealt in detail with the study of 3D cultivation of stem cells using a natural polymer, specifically alginate. In the theoretical part, the basic characteristics and possibilities of using alginate in biomedical engineering were discussed. The practical part of the work demonstrated the application of theoretical knowledge in the cultivation of stem cells from the amnion-chorion membrane in an alginate matrix.

Experiments have confirmed that alginate provides an effective environment for the growth and differentiation of stem cells, which supports their use in biomedical engineering. The overall findings of this work point to the great potential of natural polymers in biomedical applications and open the way for further research that could lead to new therapeutic strategies for the treatment of various diseases. The findings from this study show us that the 3D culture technique in alginate is an effective tool for biomedical research and tissue engineering applications. Cells cultured by this method show promising results for further experimental and therapeutic use, while their 3D arrangement greatly increases the relevance of the results for clinical applications.

Acknowledgement

The state grant agency supported this article: KEGA 018TUKE-4/2023, VEGA 1/0599/22 and APVV 22- 0340.

References

[1] ZAKRZEWSKI, W., DOBRZYNSKI, M., SZYMONOWIC, M.: Stem cells: past, present, and future, *Stem Cell Research & Therapy*, Vol. 10, No. 1, pp. 1-22, 2019. https://doi.org/10.1186/s13287-019-1165-5

[2] RAUS, R.A., NAWAWI, W.M.F.W., NASARUDDIN, R.: Alginate and alginate composites for biomedical applications, *Asian Journal of Pharmaceutical Sciences*, Vol. 16, No. 3, pp. 280-306, 2021. https://doi.org/10.1016/j.ajps.2020.10.001

[3] SAHOO, D.R., BISWAL, T.: Alginate and its application to tissue engineering, *SN Applied Sciences*, Vol. 3, No. 1, pp. 1-19, 2021. https://doi.org/10.1007/s42452-020-04096-w

[4] VENKETSAN, J., BHATNAGAR, I., MANIVASAGAN, P., KANG H., KIM, K.: Alginate composites for bone tissue engineering: A review, *International journal of biological macromolecules*, Vol. 72, pp. 269-281, 2015. https://doi.org/10.1016/j.ijbiomac.2014.07.008

[5] PAWAR, S.N., EDGAR, K.J.: Alginate derivatization: A review of chemistry, properties and applications, *Biomaterials*, Vol. 33, No. 11, pp. 3279-3305, 2012. https://doi.org/10.1016/j.biomaterials.2012.01.007

[6] BOUHADIR, K.H., LEE, K.Y., ALSBERG, E.K., DAMM, L., ANDERSON, K.W., MOONEY, D.J.: Degradation of partially oxidized alginate and its potential application for tissue engineering, *Biotechnology progress*, Vol. 17, No. 5, pp. 945-950, 2001. https://doi.org/10.1021/bp010070p

[7] SPICER, C.D.: Hydrogel scaffolds for tissue engineering: the importance of polymer choice, *Polymer Chemistry*, Vol. 11, No. 2, pp. 184-219, 2020. https://doi.org/10.1039/C9PY01021A

Review process
Single-blind peer review process.

Acta Tecnología - International Scientific Journal about Technologies
Volume: 10 2024 Issue: 2 Pages: 51-56 ISSN 2453-675X

https://doi.org/10.22306/atec.v10i2.199 Received: 05 Apr. 2024; Revised: 15 May 2024; Accepted: 27 June 2024

Using neural networks to forecast the frequency of accidents on particular Polish road types

Piotr Gorzelanczyk
Stanislaw Staszic University of Applied Sciences in Pila, Podchorazych 10 Street, 64-920 Pila, Poland, EU, piotr.gorzelanczyk@ans.pila.pl ORCID 0000-0001-9662-400X (corresponding author)
Miriam Garbarova
Faculty of Operation and Economics of Transport and Communications, University of Žilina, Univerzitná 8215/1, 010 26 Žilina, Slovak Republic, EU, miriam.garbarova@uniza.sk

Keywords: forecasting, road accident, road types, neural networks.
Abstract: Globally, the quantity of road accidents is steadily decreasing annually. Even if the epidemic has recently had an effect, this number is still quite high. Therefore, every attempt should be made to reduce this number. The purpose of this article is to forecast the number of accidents that will transpire on various kinds of roads in Poland. For this purpose, monthly data on the total number of traffic accidents in Poland broken down by type of road were examined. Based on police data, a forecast was created for the years 2022–2040. A few neural network models were used to predict the frequency of accidents in Poland. The results show that we should keep expecting a high degree of stability in terms of the quantity of traffic accidents. On the one hand, the construction of new highways and the increase in the number of cars on Polish roads have an effect on this. The number of random samples utilized in the processes of learning, testing, and validation affects the results. In the case of 70-15-15, the average projected number of accidents for 2022-2024 should be: motorway - 827, expressway - 1136, 2 one-way carriageway - 5451, single carriageway -3067 and 1 carriageway 2 directions - 28048, respectively. For 80-10-10, these values should be respectively: motorway - 1057, expressway - 1141, 2 one-way carriageway - 5486, single carriageway -2745 and 1 carriageway 2 directions - 28039. As you can see, the values are similar.

1 Introduction

A significant number of people lose their lives in traffic accidents each year. The WHO estimates that over 1.3 million people die in car crashes annually. For kids and young people between the ages of 5 and 29, traffic accidents are the leading cause of death [1]. The goal of reducing traffic-related fatalities and injuries by half by 2030 has been set by the UN General Assembly.

Many sources provide information regarding road accidents. One example is information that government organizations have obtained with the help of pertinent government entities. Data is gathered from police reports, insurance databases, and hospital records. The transportation sector's partial traffic accident data is then examined more broadly [2].

The literature has a variety of methods for accident frequency forecasting. The most often used techniques are time series methods [3,4]. However, their drawbacks include frequent residual component autocorrelation and the inability to evaluate prediction quality based on prior forecasts [5]. In contrast, Sunny et al. [6] utilized the Holt-Winters exponential smoothing method, while Procházka et al. [7] used the multiple seasonality model for forecasting. This method prevents the inclusion of exogenous variables in the model [8,9].

We can also use autoregressive models [10], regression models with curve fitting, and vector autoregressive models, which have the drawback of requiring a large number of variable observations in order to correctly estimate their parameters [11]. This is not always possible. Consequently, these just call for autoregressive order (assuming the series is already stationary) and simple linear relationships [12,13].

In their research, Chudy-Laskowska and Pisula [14] used the ANOVA approach to forecast the problem at hand. This strategy's drawback is that it necessitates the employment of additional assumptions, which when broken can lead to inaccurate findings [15]. Neural network models are also used to estimate the amount of traffic accidents. This strategy's drawback is that it necessitates a fundamental comprehension of the subject [16]. Furthermore, because SNF is frequently referred to as a "black box," in which input is provided and the model provides findings without knowledge of the analysis, the forecast result is dependent on the adoption of the network's beginning conditions as well as the inability of traditional interpretation [17].

Using the previously provided statistics, the author made estimates for the quantity of accidents that would occur on Polish roads. Neural networks were used to forecast how many accidents would occur.

2 Materials and methods

Every year, a number of incidents occur on Polish roads. Recent years have seen a decrease in road accidents due to the epidemic, which affects the estimated value that

was established. Despite the epidemic, there are still a lot of road accidents. As a result, every attempt should be made to reduce this figure and determine the types of routes where most accidents will take place (Figure 1). Most traffic accidents occur on highways having a single carriageway that runs in both directions.

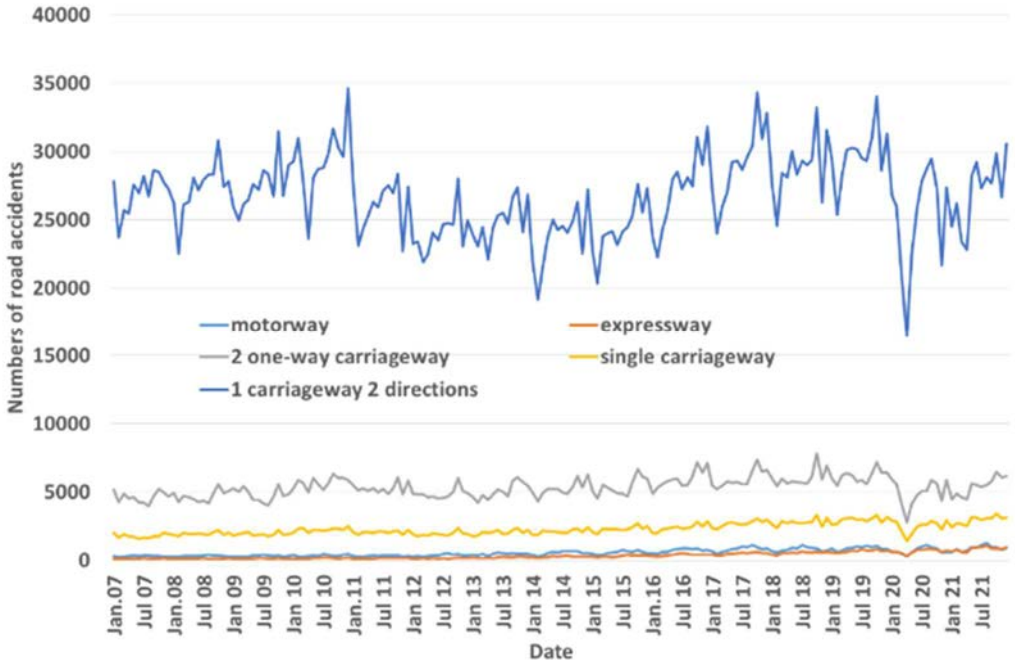

Figure 1 Number of road accidents in Poland by road type in 2007-2021 [18]

Different neural network models were used to predict the number of accidents that will occur on Polish roads based on the kind of road. The advantage of this method is that it mimics the way the human brain works. Neural networks are composed of nodes, each of which has inputs, weights, variances, and outputs. The optimal weights for the study were selected by the Statistica software. The result of predicting using the previously discussed method will depend on the model and its parameters that are chosen.

Using the forecasting mistakes obtained from equations (1-5), the following metrics of analytical forecasting brilliance were calculated:

- ME – mean error

$$ME = \frac{1}{n}\sum_{i=1}^{n}(Y_i - Y_p) \quad (1)$$

- MAE – mean error

$$MAE = \frac{1}{n}\sum_{i=1}^{n}|Y_i - Y_p| \quad (2)$$

- MPE – mean percentage error

$$MPE = \frac{1}{n}\sum_{i=1}^{n}\frac{Y_i - Y_p}{Y_i} \quad (3)$$

- MAPE - mean absolute percentage error

$$MAPE = \frac{1}{n}\sum_{i=1}^{n}\frac{|Y_i - Y_p|}{Y_i} \quad (4)$$

- SSE – mean square error

$$SSE = \sqrt{\frac{1}{n}\sum_{i=1}^{n}(Y_i - Y_p)^2} \quad (5)$$

where:
n – length of forecast horizon,
Y – observed value of road accidents,
Y_p – forecasting value of road accidents.

Neural network models with the least mean absolute percentage error and mean percentage error were used to forecast the frequency of traffic accidents by type of road.

3 Results

To look into the temporal evolution of the accident rate on different kinds of roads, the Kruskall-Wallis test was used. 830 is the test statistic, while 0.000 is the test probability. The result shows that we do not take the mean number of traffic accidents to be equal (Figure 2).

Using neural networks to forecast the frequency of accidents on particular Polish road types
Piotr Gorzelanczyk, Miriam Garbarova

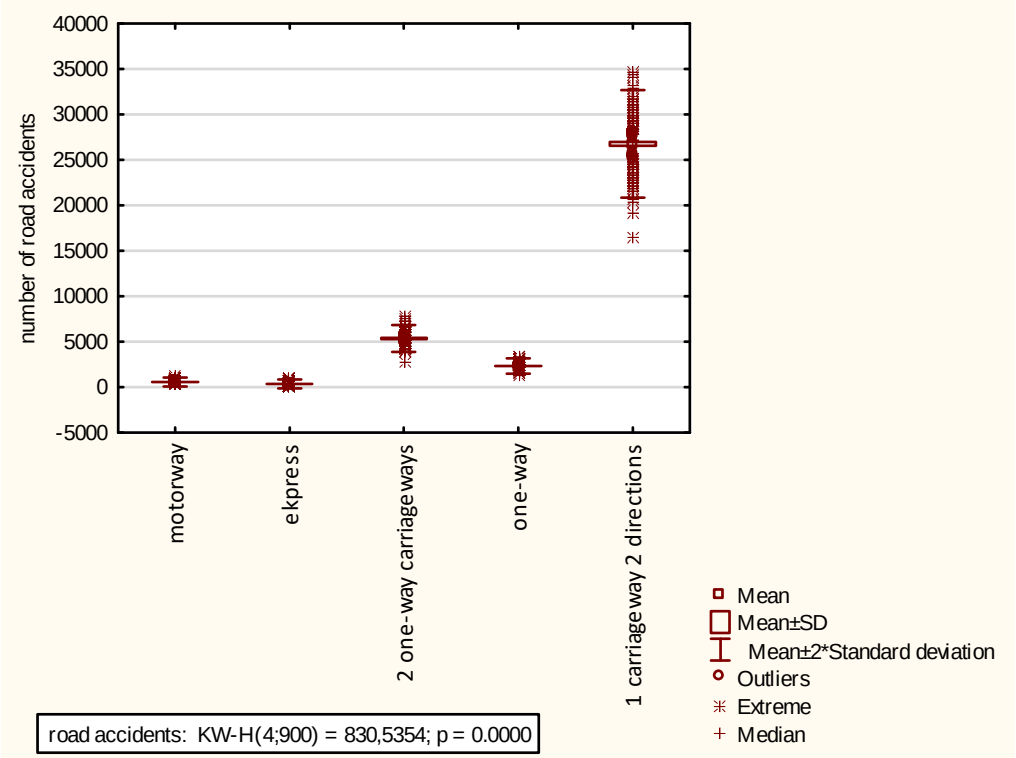

Figure 2 Comparison of the average number of road accidents in Poland by road type from 2007 to 2021 [18]

Using data from the Polish Police from 2007 to 2021, the annual number of traffic accidents in Poland was estimated based on the kind of route [18]. Two random sample sizes were assumed when the study was carried out using Statistica software:

- 70% is education, 15% testing, and 15% validation.
- 80% of instruction, 10% testing, and 10% validation.

With 20, 40, 60, 80, 100, 200 learning networks, for which the MP error value was negligible (Table 1, Table 2).

Table 1 Neural network learning summary for the random sample size case teaching 70%, testing 15% and validation 15%

Type of road	Network number	Network name	Quality (learning)	Quality (learning)	Quality (validation)	Learning algorithm	Activation (hidden)	Activation (output)	Errors				
									ME	MAE	MPE	MAPE	SSE
motorway	200	MLP 12-5-1	0.925071	0.937989	0.971657	BFGS 10	Logistics	Linear	9.56597754	63.36167	0.46 %	11.83 %	88.49127
expressway	20	MLP 12-7-1	0.951552	0.974197	0.975260	BFGS 7	Linear	Linear	8.01655915	44.85012	0.33 %	13.65 %	67.75909
2 single carriageways	20	MLP 12-5-1	0.689403	0.719414	0.873958	BFGS 9	Tanh	Logistics	53.456 7291	378.2578	0.00 %	7.21%	521.1392
one-way	40	MLP 12-4-1	0.883924	0.898429	0.938170	BFGS 61	Tanh	Logistics	13.570 2339	133.3945	0.05 %	5.81%	187.7956
1 carriageway 2 directions	60	MLP 12-8-1	0.869698	0.808519	0.700377	BFGS 61	Logistics	Linear	85.878 5093	1249.393	0.02 %	4.80%	1679.773

Table 2 Neural network learning summary for the random sample size case teaching 80%, testing 10% and validation 10%

Type of road	Network number	Network name	Quality (learning)	Quality (learning)	Quality (validation)	Learning algorithm	Activation (hidden)	Activation (output)	Errors				
									ME	MAE	MPE	MAPE	SSE
motorway	40	MLP 12-7-1	0.898808	0.914107	0.950540	BFGS 4	Linear	Logistics	18.412 4803	79.69277	0.05 %	14.77%	106.1922
expressway	20	MLP 12-3-1	0.961444	0.977631	0.980714	BFGS 6	Linear	Linear	8.10325895	40.83375	0.55 %	12.39%	61.32151
2 single carriageways	20	MLP 12-5-1	0.681920	0.831358	0.873351	BFGS 6	Linear	Tanh	48.140 1442	379.1432	0.06 %	7.26%	521.4526
one-way	200	MLP 12-2-1	0.835982	0.897177	0.956450	BFGS 13	Logistics	Tanh	21.371 6664	159.9512	0.03 %	6.95%	217.5564
1 carriageway 2 directions	200	MLP 12-7-1	0.841886	0.797305	0.738706	BFGS 31	Tanh	Exponential	117.84 3275	1345.519	0.06 %	5.12%	1713.832

Regardless of the type of road, Poland's annual rate of traffic accidents is likely to stabilize at a high level based on the research findings. The results are impacted by the random sample size selection. By increasing the proportion of the learning group compared to the test and validation group, the average percentage error is decreased.

During a learning group of 70%, test group of 15%, and validation group of 15% (70-15-15), the error was 13.65%; however, during the second test (80-10-10) the error was 14.7%. For highways, which are showing up on Poland's map more frequently every year. It is important to note that the outbreak affected the results (Figure 3, Figure 4).

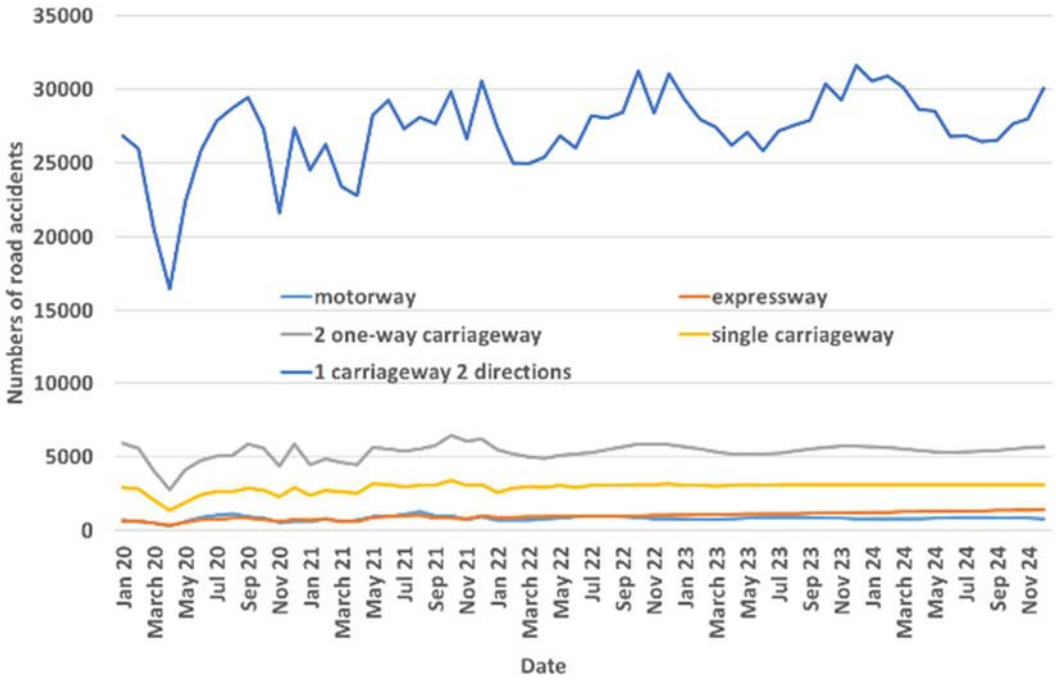

Figure 3 Forecasting number of road accidents for 2022-2024 for the 70-15-15 test group

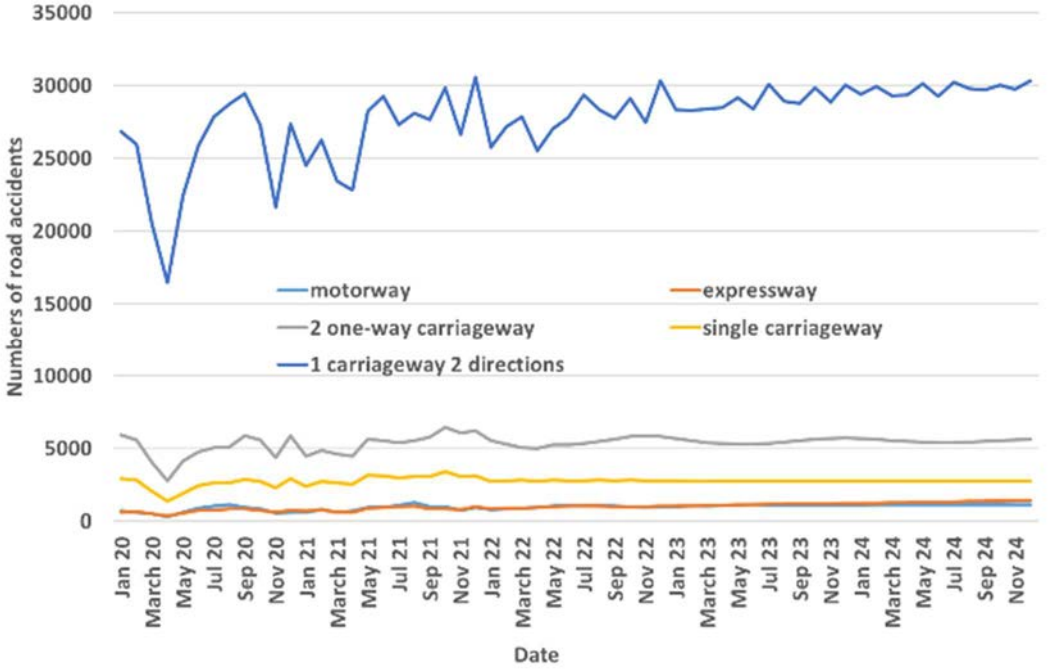

Figure 4 Forecasting number of road accidents for 2022-2024 for the 80-10-10 test group

4 Conclusion

The research utilized neural networks in the Statistica environment to predict the frequency of accidents in Poland based on the kind of road. The research's weights were assessed by the computer in order to reduce both the mean absolute error and the mean absolute percentage error.

The statistics makes it evident that there is still a chance for the number of traffic accidents to stabilize. This is affected, on the one hand, by the growth of motorways and the increase in the quantity of automobiles on Polish roads. The estimated forecasting errors show that the models that were utilized are valid.

Based on the derived projections, steps should be taken to further minimize the number of traffic accidents. Among these modifications might be the imposition of higher fines for moving offenses starting on January 1, 2022, on Polish roads. The epidemic surely affected the study's conclusions because it drastically decreased the number of accidents on the roads.

In the case of 70-15-15, the average projected number of accidents for 2022-2024 should be: motorway - 827, expressway - 1136, 2 one-way carriageway - 5451, single carriageway - 3067 and 1 carriageway 2 directions - 28048, respectively. For 80-10-10, these values should be respectively: motorway - 1057, expressway – 1141 , 2 one-way carriageway - 5486, single carriageway -2745 and 1 carriageway 2 directions - 28039. As you can see, the values are similar.

The authors want to include other variables that influence accident frequency and use alternative statistical methods to determine the total number of collisions in their follow-up study. These could include factors like the volume of traffic, the kind of weather, the age of the driver, and methods that compute accident frequency using exponential growth.

References

[1] WHO, The Global status on road safety, [Online], Available: https://www.who.int/publications/i/item/9789241565684 [02 Apr 2024], 2018.

[2] GORZELANCZYK, P., PYSZEWSKA, D., KALINA, T., JURKOVIC, M.: Analysis of road traffic safety in the Pila poviat, *Scientific Journal of Silesian University of Technology*, Series Transport, Vol. 107, pp. 33-52, 2020. https://doi.org/10.20858/sjsutst.2020.107.3

[3] HELGASON, A.F.: Fractional integration methods and short Time series: evidence from asimulation study, Political Analysis, Vol. 24, No. 1, pp. 59-68, 2016. https://doi.org/10.1093/pan/mpv026

[4] LAVRENZ, S.M., VLAHOGIANNI, E.I., GKRITZA, K., KE, Y.: Time series modeling in traffic safety research, *Accident Analysis & Prevention*, Vol. 117, pp. 368-380, 2018. https://doi.org/10.1016/j.aap.2017.11.030

[5] Forecasting based on time series, [Online], Available: http://pis.rezolwenta.eu.org/Materialy/PiS-W-5.pdf [02 Apr 2024], 2022. (Original in Polish)

[6] SUNNY, C.M., NITHYA, S., SINSHI, K.S., VINODINI, V.M.D., LAKSHMI, A.K.G., ANJANA, S., MANOJKUMAR, T.K.: *Forecasting of Road Accident in Kerala: A Case Study*, 2018 International Conference on Data Science and Engineering (ICDSE), Kochi, India, pp. 1-5, 2018. https://doi.org/10.1109/ICDSE.2018.8527825

[7] PROCHÁZKA, J., FLIMMEL, S., ČAMAJ, M., BAŠTA, M.: *Modelling the Number of Road Accidents*, 20th AMSE, Applications of Mathematics and Statistics in Economics, International Scientific Conference: Szklarska Poręba, 30 August - 3 September 2017, Conference Proceedings Full Text Papers, Publishing house of the University of Economics in Wrocław, Wrocław, pp. 355-364, 2017. https://doi.org/10.15611/amse.2017.20.29

[8] DUDEK, G.: *Forecasting Time Series with Multiple Seasonal Cycles Using Neural Networks with Local Learning*, In: Rutkowski, L., Korytkowski, M., Scherer, R., Tadeusiewicz, R., Zadeh, L.A., Zurada, J.M. (eds) Artificial Intelligence and Soft Computing, ICAISC 2013, Lecture Notes in Computer Science, Vol. 7894, Springer, Berlin, Heidelberg, 2013. https://doi.org/10.1007/978-3-642-38658-9_5

[9] SZMUKSTA-ZAWADZKA, M., ZAWADZKI, J.: Forecasting on the basis of Holt-Winters models for complete and incomplete data, *Ekonometria*, Vol. 24, No. 38, pp. 85-99, 2009. (Original in Polish)

[10] MONEDEROA, B.D., GIL-ALANAA, L.A., MARTÍNEZAA, M.C.V.: Road accidents in Spain: Are they persistent?, *IATSS Research*, Vol. 45, No. 3, pp. 317-325, 2021. https://doi.org/10.1016/j.iatssr.2021.01.002

[11] WÓJCIK, A.: *Autoregressive vector models as a response to the critique of multi-equation structural econometric models*, Publishing house of the University of Economics in Katowice, Katowice, 2014.

[12] MAMCZUR, M.: Machine learning How does linear regression work? And is it worth using?, [Online], Available: https://miroslawmamczur.pl/jak-dziala-regresja-Linear-i-czy-warto-ja-stosowac [02 Apr 2024], 2024.

[13] PIŁATOWSKA, M.: The choice of the order of autoregression depending on the parameters of the generating model, *Econometrics*, Vol. 4, No 38, 2012.

[14] CHUDY-LASKOWSKA, K., PISULA, T.: Forecasting the number of road accidents in Subcarpathia, *Logistics*, Vol. 4, pp. 2782-2796, 2015. (Original in Polish)

[15] GREGORCZYK, A., SWARCEWIC, M.: Analysis of variance in a system of repeated measurements to determine the effects of factors influencing linuron

residues in soil, *Polish Journal of Agronomy*, Vol. 11, pp. 15-20, 2012. (Original in Polish)

[16] CHUDY-LASKOWSKA, K., PISULA, T.: Forecast of the number of road accidents in Poland, *Logistics*, Vol. 6, pp. 2710-2721, 2014. (Original in Polish)

[17] Data mining techniques StatSoft, [Online], Available: https://www.statsoft.pl/textbook/stathome_stat.html?https%3A%2F%2Fwww.statsoft.pl%2Ftextbook%2Fstdatmin.html [02 Apr 2024], 2024.

[18] Statistic Road Accident, [Online], Available: https://statystyka.policja.pl [02 Apr 2024], 2023. (Original in Polish)

Review process
Single-blind peer review process.

Acta Tecnología - International Scientific Journal about Technologies
Volume: 10 2024 Issue: 2 Pages: 57-64 ISSN 2453-675X

https://doi.org/10.22306/atec.v10i2.200 Received: 06 Apr. 2024; Revised: 12 May 2024; Accepted: 29 May 2024

Investigating the feasibility of energy harvesting from the third pedal in automotive systems using a mechanical motion rectifier: simulation-based study

Mohammed Alaa Alwafaie
István Sályi Doctoral School of Mechanical Engineering Sciences, Egyetem út 1, 3515, Miskolc, Hungary, EU, alwafaie.mohammad.alaa@student.uni-miskolc.hu (corresponding author)
Bela Kovacs
István Sályi Doctoral School of Mechanical Engineering Sciences, Egyetem út 1, 3515, Miskolc, Hungary, EU, matmn@uni-miskolc.hu

Keywords: energy harvesting, mechanical motion rectifier, simulation, electrical power generation.
Abstract: Automotive vehicles provide opportunities for energy harvesting from the mechanical motion generated during driving. In this study, we propose a novel design for a mechanical motion rectifier (MMR) that can generate electrical power from the mechanical motion of the third pedal in manual transmission vehicles. Using simulation and design tools, we investigate the feasibility of this system and explore the potential benefits and challenges of implementing it in automotive vehicles. Our results show that the proposed MMR system can effectively convert the oscillatory motion of the third pedal into unidirectional motion, which can then be used to generate electrical power. We also demonstrate that the design and operating parameters of the MMR system significantly impact its efficiency and performance. Our findings provide insights into the design and optimization of MMR systems for energy harvesting in automotive vehicles and highlight the potential for this technology to contribute to sustainable energy solutions.

1 Introduction

The quest for environmentally friendly and cost-effective energy solutions has fueled considerable improvements in the field of energy harvesting. Energy harvesting from mechanical motion has gained popularity as a possible method of producing electrical power in a variety of applications. The mechanical motion caused by driving gives an opportunity to utilize this energy source in the context of automobiles [1-3]. While driving, the third pedal frequently oscillates when pressure is applied to either the brake pedal or the throttle pedal. This oscillation is caused by a rod that connects both pedals. If effectively converted into electrical power, this movement could serve as a supplementary or alternative power source for automotive systems. The figure 1 shows a schematic of the mechanical motion transformation MMR for the third pedal [4].

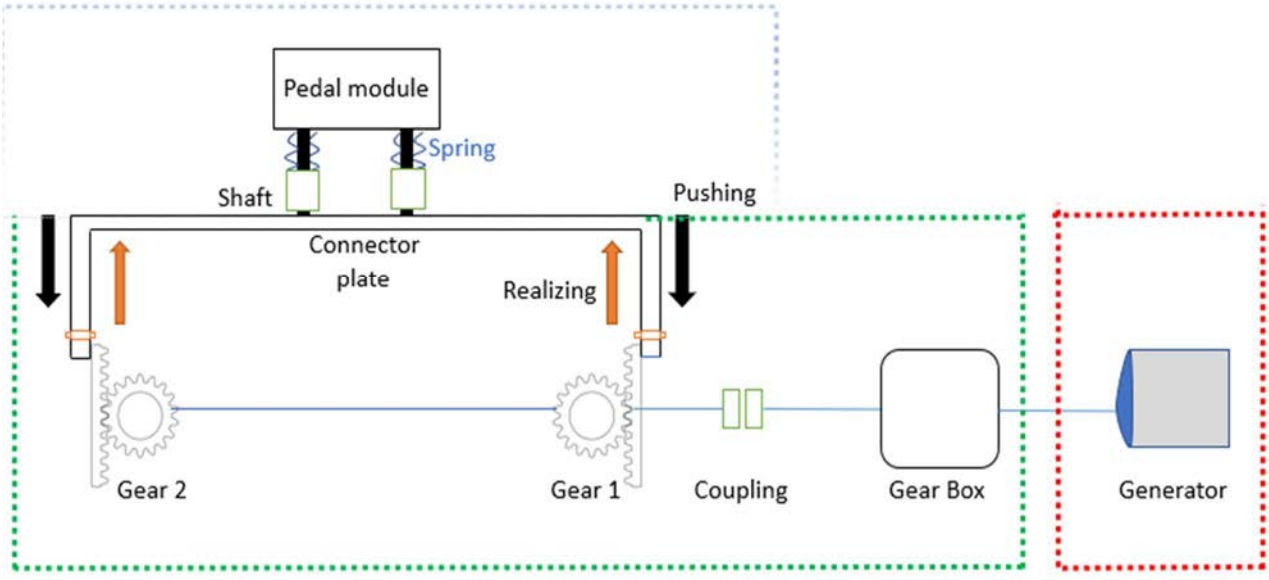

Figure 1 A schematic of the mechanical motion transformation MMR for the third pedal [4]

Investigating the feasibility of energy harvesting from the third pedal in automotive systems using a mechanical motion rectifier: simulation-based study

Mohammed Alaa Alwafaie, Bela Kovacs

The MMR achieves the conversion of linear motion from racks into rotational motion by interlocking pinion gears 1 and 2. When the driver vertically presses the pedal module, the rack moves, causing the pinion gear to rotate and the shaft to spin. This rotation of the shaft drives the gearbox, which in turn rotates the DC motor, generating electric power. To enhance power generation efficiency, a gearbox is utilized to increase rotational speed, as the linear motion of the rack alone cannot achieve high speeds. The generated energy is stored in a battery and can be used to recharge the vehicle at a later time.

2 Statistical analysis

To start statistical modeling, it is better to have an understanding of the various dynamics of the mechanical motion transformer MMR. This is crucial in investigating the feasibility of energy harvesting from the third pedal and demonstrating how we can control and extract power from this strategy.

2.1 Pedal harvesting energy dynamics

Pedal harvesting energy is a concept that involves utilizing the mechanical motion of a pedal, such as in a vehicle or a bicycle, to generate and harvest energy. In this context, the pedal serves as a means to convert mechanical force into usable energy [5-10].

Figure 2 illustrates the system of pedal harvesting energy, highlighting the pressed force acting on the pedal (PHE). This force is typically applied by the user, whether through their foot or another means of interaction. Understanding how this force is transmitted and translated within the system is crucial in analyzing the dynamics of pedal harvesting energy. It is important to understand how the pedal interacts with the mechanical motion transformer (MMR) as it plays a key role in determining the torque exerted on it.

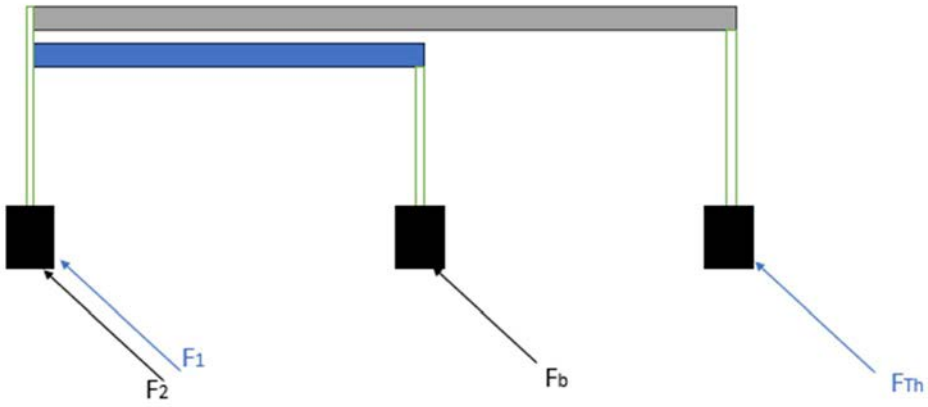

$F_{b:}$ The pressed force from the brake pedal,
F_{Th}: The pressed force from the throttle pedal,
F_1 & F_2: Forces that come from pressing the throttle and brake pedals separately.

Figure 2 The pressed force acting on the pedal (PHE)

The connection between the PHE (Pedal Harvesting Energy) system and the MMR (Mechanical Motion Transformer) system can be established through the consideration of spring stiffness and equivalent electrical damping as shown in figure 3. Spring stiffness K_b refers to the stiffness or resistance offered by a spring when it is compressed or stretched. In the context of the PHE and MMR system, the spring stiffness can be used to control the interaction between the pedal and the mechanical motion transformer. It determines the amount of force required to compress or stretch the spring, thereby affecting the torque and power transmission within the system. Equivalent electrical damping C_b refers to the damping effect that can be represented by an electrical circuit equivalent to the mechanical system. It is used to model the dissipation of energy within the system due to factors such as friction, air resistance, or other forms of mechanical damping.

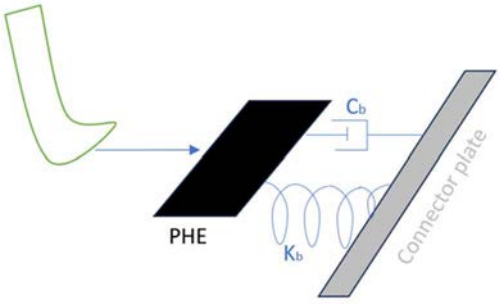

Figure 3 The connection between the PHE and the MMR by C_b, K_b

Investigating the feasibility of energy harvesting from the third pedal in automotive systems using a mechanical motion rectifier: simulation-based study

Mohammed Alaa Alwafaie, Bela Kovacs

By incorporating equivalent electrical damping, the behavior and response of the system can be analyzed and optimized. The spring stiffness and equivalent electrical damping are parameters that can be adjusted and optimized to achieve desired performance characteristics in the PHE and MMR system. They play a role in determining factors such as the system's response time, stability, energy efficiency, and overall performance [11-14].

Based on Newton's second law of motion, we can write the equation of motion for the PHE (Pedal Harvesting Energy) system as follows (1), (2):

$$Mb\,.\,\ddot{x} + Cb\,.\,\dot{x} + kb.x = F_1 + F_2 \quad (1)$$

$$Mb\,.\,\ddot{x} + Cb\,.\,\dot{x} + kb.x = F_t \quad (2)$$

2.2 Dynamics equations for rack in MMR

The dynamic's equation for rack may describe based on Newton second law and according on figure 4 as follow (3), (4):

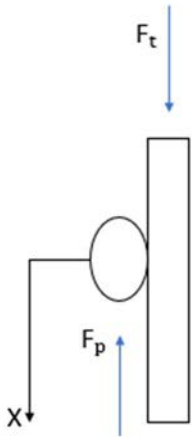

Figure 4 The forces acting on rack of MMR

$$M_r\,.\,a = F \quad (3)$$

$$M_r\,.\,\ddot{x} = -F_p + F_t \quad (4)$$

Also, the force of pinion gear can give as (5), (6):

$$F_p = \frac{2\pi T_p}{p\,\eta\,R} = K\frac{T_p}{R} \quad (5)$$

T_p: torque of pinion gear,
P: pitch of pinion,
η: efficiency of pinion,
R: the radius of pinion.

$$M_r\,.\,\ddot{x} + K\frac{T_p}{R} = F_t \quad (6)$$

2.3 Dynamics equations for pinion and outer ring of one-way clutch in MMR

In order to determine the equation for the given situation involving the MMR (Multi-Mass Rotor), it is necessary to sketch the torques and inertia associated with the system. To begin, a sketch of the MMR should be created, clearly indicating the positions of the angular displacement and the axis of rotation as in figure 5.

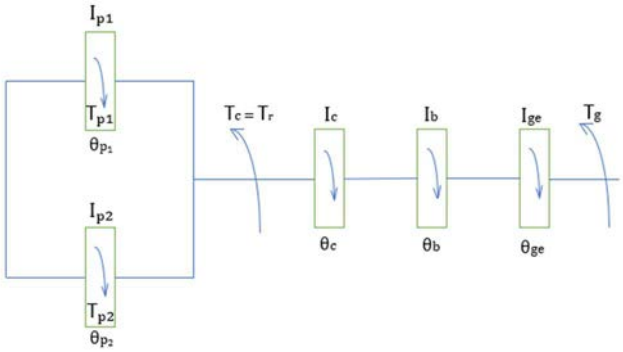

Figure 5 The moment of inertia and torques of MMR

Next, the moment of inertia for the MMR must be considered. The moment of inertia represents the rotational inertia of the system and is influenced by the distribution of masses and their distances from the axis of rotation. The total moment of inertia for the MMR can be obtained by summing the individual moments of inertia for each mass (7).

$$I = \int r^2.dm \quad (7)$$

dm: Differentiation mass for each part,
r: Distance for each part from axis of rotation.

The equation for the given situation can be derived by applying Newton's second law for rotational motion. This equation relates the net torque acting on the system to the moment of inertia and the angular acceleration of the MMR, so that for pinion allows us to analyze the rotational dynamics as follows (8), (9):

$$I_{p,n}\,.\,\ddot{\theta}_{p,n} = T_p - T_r \quad (8)$$

n = 1.2 because we have here in this case only two pinion gear.
$T_r = T_c$: The prevents rotation torque due to the presence of external loads or disturbances acting on the ring.

$$I_{p,n}\,.\,\ddot{\theta}_{p,n} = T_p - Tc \quad (9)$$

For the ring (10):

$$I_0\,.\,\ddot{\theta}_0 = -T_p \quad (10)$$

2.4 Dynamics equations for coupling, gearbox and generator in MMR

Depending on the moment of inertia and figure 5 we can determine each of dynamic equations for (11), (12):

1- Coupling

$$Ic\,.\,\ddot{\theta}c = Tc \quad (11)$$

2- Gearbox and generator

$$Ige\,.\,\ddot{\theta}ge + Ic\,.\,\ddot{\theta}c = Tc - Tg \quad (12)$$

$\theta_c = \theta_b = \theta$, $\theta_{ge} = n.\theta_b$ (n the ratio of gearbox) we can write (13):

$$Ige\,.n.\ddot{\theta}b + Ic\,.\ddot{\theta}b = Tc - Tg$$
$$(Ige\,.n + Ic\,)\ddot{\theta}b = Tc - Tg \quad (13)$$

Electromagnetic induced torque (T_g):

This torque produced by the interplay of electric currents and magnetic fields in a spinning electrical machine, such as generator and it gives as (14):

$$Tg = K_t\,.B\,.I.\sin\alpha \quad (14)$$

K_t is a constant factor that depends on the specific design of the machine.
B represents the strength of the magnetic field.
I represent the current flowing through the machine.
α is the angle between the magnetic field and the current.

In a simplified design scenario where there is a linear relationship between the torque and current, we can set α to 90° (indicating that the magnetic field and current are perpendicular) and assume B to be equal to 1 (representing a unit magnetic field strength). In this simplified case, the equation for the torque becomes (15):

$$Tg = K_t\,.I \quad (15)$$

This simplified design allows for a straightforward relationship between the torque and current, where the torque is directly proportional to the current. However, it's important to note that in practical electrical machines, the relationship between torque and current can be more complex and dependent on various factors such as the machine's design, magnetic field strength, and operating conditions.

From each of equations 6,9,13 we can analysis the equation for harvesting energy as following (16)-(23):

$$M_r\,.\ddot{x} + K\frac{T_p}{R} = F_t \quad (16)$$
$$M_r\,.r.\ddot{\theta} + K\frac{T_p}{R} = F_t \quad (17)$$
$$I_{p,n}\,.\ddot{\theta}_{p,n} = T_p - Tc \quad (18)$$
$$T_p = I_{p,n}\,.\ddot{\theta}_{p,n} + Tc \quad (19)$$
$$(Ige\,.n + Ic\,)\ddot{\theta}b + Tg = Tc \quad (20)$$
$$T_p = I_{p,n}\,.\ddot{\theta} + (Ige\,.n + Ic\,)\ddot{\theta} + Tg \quad (21)$$
$$T_p = (I_{p,n} + Ige\,.n + Ic\,)\ddot{\theta} + Tg \quad (22)$$
$$M_r\,.r.\ddot{\theta} + \frac{K}{R}(I_{p,n} + Ige\,.n + Ic\,)\ddot{\theta} + \frac{K}{R}.Tg = F_t \quad (23)$$

From equation 15 we can write (24):

$$M_r\,.r.\ddot{\theta} + \frac{K}{R}(I_{p,n} + Ige\,.n + Ic\,)\ddot{\theta} + \frac{K}{R}.K_t\,.I = F_t \quad (24)$$

The voltage (V) and current (I) for generator:

The electromotive voltage (EMF) in generator which connected by gearbox express by (25):

$$E = V = Kg.N.B.A.\omega \quad (25)$$

K_g: gear ratio and it is equal to n.
N: the number turn of coil inside the generator.
A: the area of coil.
ω: the out speed from gearbox.

We can express the voltage in another formula (26):

$$V = n.N.\dot{\theta} \quad (26)$$

Also, the current can write as (27)-(32):

$$I = V/R_t \quad (27)$$
$$I = \frac{n.N.\dot{\theta}}{R_t} \quad (28)$$
$$M_r\,.r.\ddot{\theta} + \frac{K}{R}(I_{p,n} + Ige\,.n + Ic\,)\ddot{\theta} + \frac{K}{R}.K_t\,.\frac{n.N.\dot{\theta}}{R_t} = F_t \quad (29)$$
$$[M_r\,.r + \frac{K}{R}(I_{p,n} + Ige\,.n + Ic\,)]\ddot{\theta} + [\frac{K.K_t\,.n.N}{R.R_t}]\dot{\theta} = F_t \quad (30)$$
$$M_e\,.\ddot{\theta} + C_e\,.\dot{\theta} = F_t \quad (31)$$
$$\ddot{\theta} = \frac{1}{M_e}F_t - \frac{C_e}{M_e}.\dot{\theta} \quad (32)$$

2.5 *The state of disengagement equation*

Upon disengagement of a system, the mechanical linkage between the driving force and the generator shaft is disrupted. Consequently, the generator shaft persists in its rotational motion owing to its inertia, although this motion experiences a progressive decay as time elapses. So, the angular displacement of the generator can describe as (33):

$$\dot{\theta}ge = \dot{\theta}ge\,.e^{-\alpha t} \quad (33)$$

$\alpha = C_e/M_e$ it is the decay factor, also known as the angular damping coefficient, controls the rate at which the generator shaft's rotational motion decreases.
t: this is the amount of time that has passed since the system was disconnected. The decay effect causes the angular displacement to decrease with time.

Based on equations (1), (32) and (33), it has been determined that the harvesting of energy can be achieved. The power can be calculated either from the angular velocity ($\dot{\theta}$) or from the linear velocity ($\dot{x}$) as follows (34):

$$P = Tg\,.\dot{\theta} = K_t\,.I\,.\dot{\theta} = K_t\,.I\,.\dot{x}/R = C_e\,.\dot{\theta}^2 \quad (34)$$

3 Modeling and experiment of MMR

To evaluate the effectiveness of MMR, an initial study was conducted to harvest energy from this technology. Additionally, to identify the factors that influence this energy harvest, it is necessary to determine the variable factors [15-17]. From the equation (1) we can found the pedal position as (35):

$$\ddot{x} = \frac{1}{Mb}F_t - \frac{Cb}{Mb}\dot{x} - \frac{kb}{Mb}x \quad (35)$$

Investigating the feasibility of energy harvesting from the third pedal in automotive systems using a mechanical motion rectifier: simulation-based study

Mohammed Alaa Alwafaie, Bela Kovacs

From the ODE45 and also drawing the Simulink for two equation we can found as figure 6.

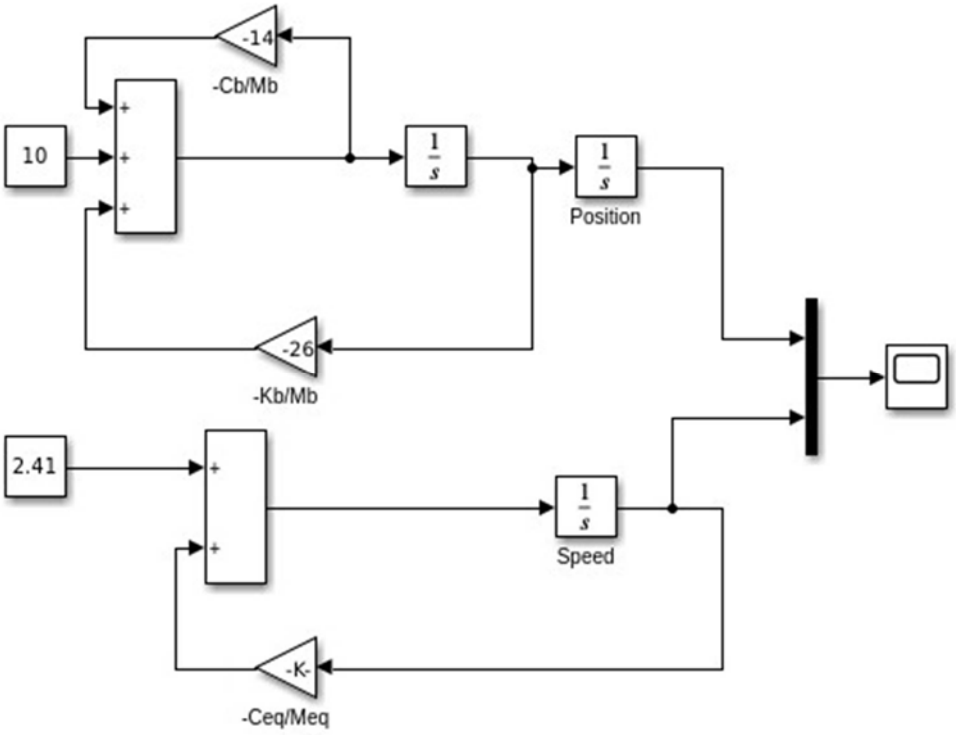

Figure 6 The drawing of Simulink for equation 1&32

The gain block comes from the indicators in the schedule (Table 1).

$$F_t = \mathrm{Mb} \cdot g \quad (36)$$

Table 1 The indicators for PHE

Name	Notation	Value and unit
Equivalent mass	Meq	207.25 kg
Pressing mass	Mb	50 kg
Equivalent coefficient when R_t =202Ω	Ceq	28.65 (N-s/m)
Pinion stiffness	K	0.5024 (N/m)
Generator stiffness	Kt	0.18 (N/m)
PHE stiffness	Kb	1300 (N/m)
PHE coefficient	Cb	700 (N-s/m)

Since (Ft) is related through (Mb) between the brake pedal and the throttle pedal according to equation (36), the value of each can be found according to scheme (Table 2).

Table 2 The value of each brake and throttle pedal in small and big cars

Type	Small or family car	Big car
Brake pedal	(23- 45) kg	(45-68) kg
Throttle pedal	(9-23) kg	(23-45) Kg

To assess the effectiveness of MMR, an initial study was conducted to investigate the energy harvesting capabilities of this technology. Furthermore, in order to determine the factors that impact this energy harvest, specific values need to be identified. As depicted in Figure 7, the signals indicating the position of the pedal and the angular speed were examined over a period of approximately 60 seconds (one minute). The analysis revealed that the position of the pedal exhibited a linear relationship with time, steadily increasing. Conversely, the angular speed showed a gradual increase until reaching a peak of 17.5 radians.

Investigating the feasibility of energy harvesting from the third pedal in automotive systems using a mechanical motion rectifier: simulation-based study

Mohammed Alaa Alwafaie, Bela Kovacs

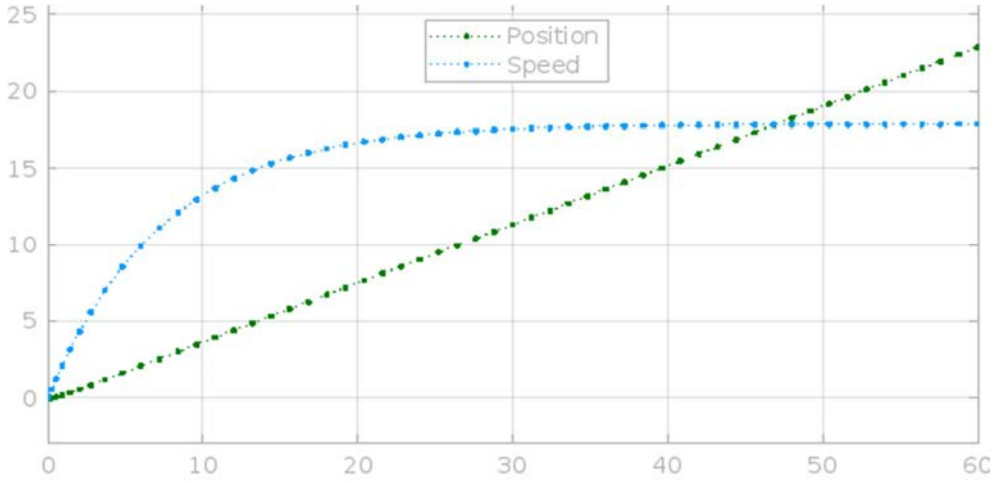

Figure 7 The position and angular speed plots to time

We can then perform a simulation according to equation (33) between the generator shaft in the left figure 8 and the pinion gear in the right figure 8 using six seconds of angular velocity (in radians) for two speed 3.21& 8.04 KMH of car speed (Figure 9).

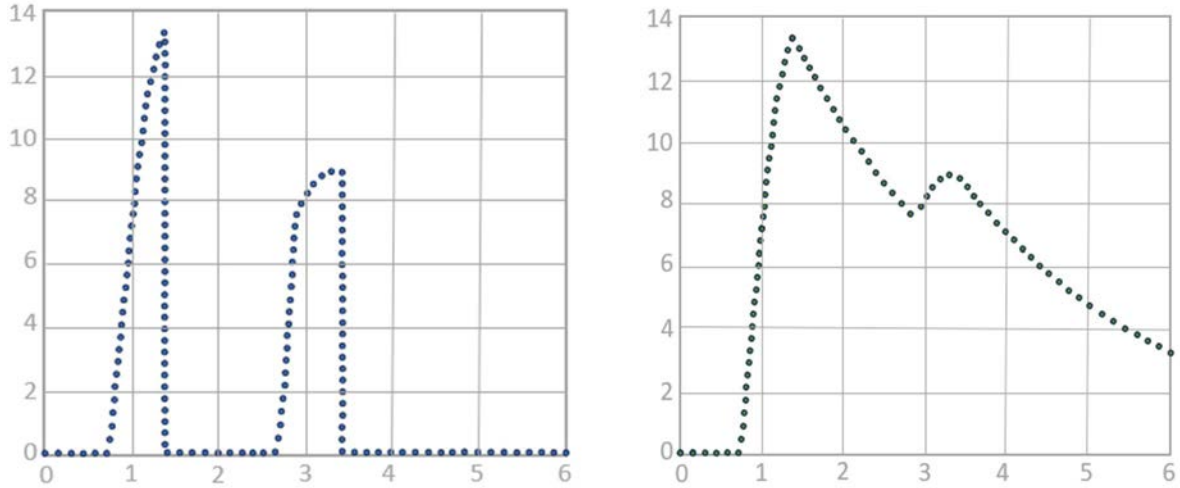

Figure 8 The position and angular speed plots to time for 3.21KMH of car speed

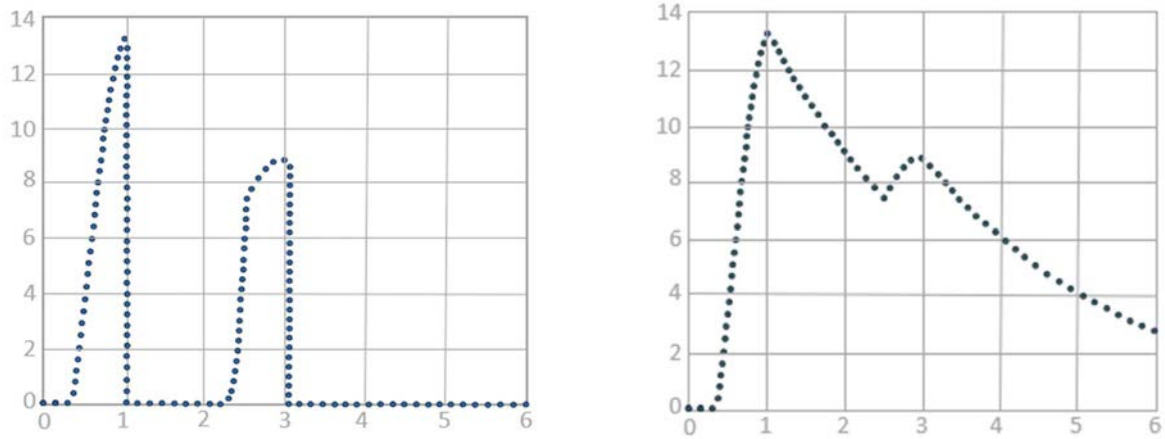

Figure 9 The position and angular speed plots to time for 8.04 KMH of car speed

The process of association and MMR dissociation is clearly visible in pervious graphs. As the vehicle begins to accelerate on the throttle pedal, the PHE descends and touches the rack and pinion assembly. Therefore, the system uses a pinion gear that drives the generator shaft at the same angular velocity. Once the lower limit of the rack is reached, the pinion releases and its angular velocity suddenly decreases to zero. After that, the system cuts off and the generator shaft continues to rotate with the decay factor (α) according to equation 33.

Since the generated power is directly proportional to the square of the angular velocity of the generator shaft, the same trend is followed the second peak observed in the figure indicated that the system engaged in retrieval process. Another thing we notice here is that as the speed of the car increases, the peaks will get closer. This makes sense because, at high speeds, the person's foot stays on the throttle pedal and moves lower and lower. So, the closure coming to the summit is a validation of that. Also pressing the brake pedal will be done when there is an emergency that needs to be pressed and using the same procedure as described before. on 202Ω we can found the power in figure 10.

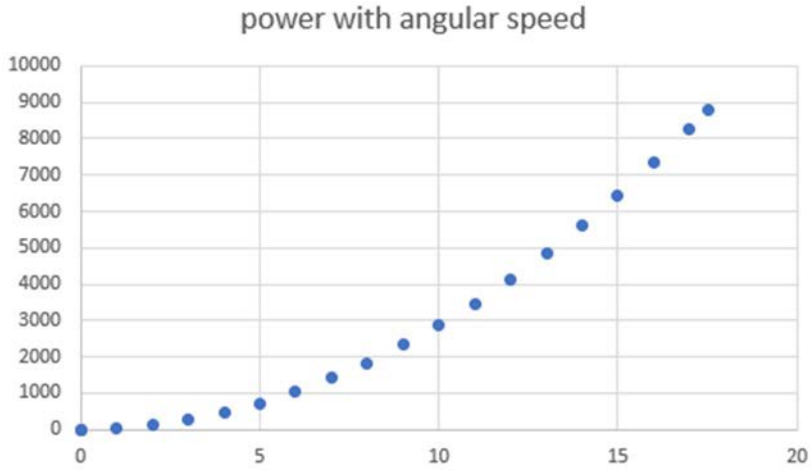

Figure 10 The power with angular speed at 202 Ω

The effect of external loads on energy production will support the simulation. To determine the energy harvested by this method it is advisable to test the different resistance connected to the generator as it gives us knowledge about the current. The simulation was conducted at a speed of 11.26 -16.09 km/h. We saw in figure 11 that we have two of the pressure peaks at PHE and generating power for R=110 Ω gives about 1145 watts for the first peak and about 735 watts for the second peak.

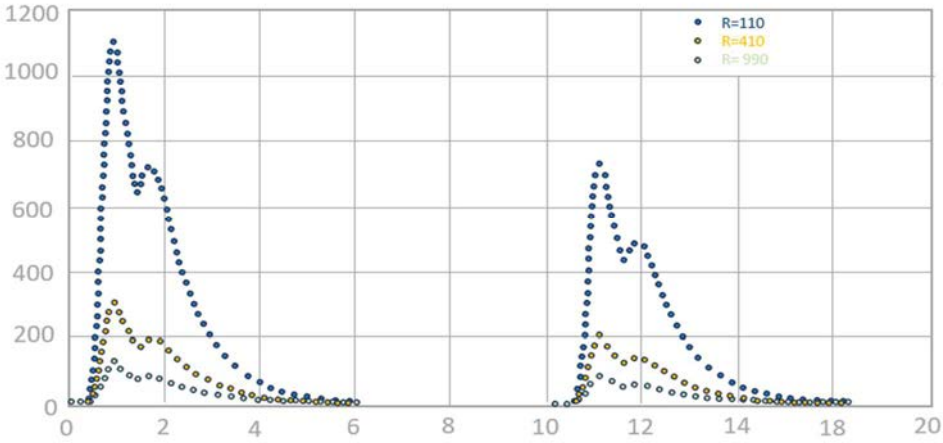

Figure 11 The generating power with time and different resistance

4 Conclusion

In this work, alternative energy harvesting has been investigated and developed using scientific method and technique. The pedal harvester and its geometry have been thoroughly studied, and a method for large scape electrical harvesting has been proposed. The ability of the pedal

energy harvester to generate electricity is determined by simulations field tests A MATLAB model has been developed to analyze the simulation results and the developed pedal energy harvester prototype has the ability to approximate 1100 watts of peak current. The proposed pedal power collector is expected to provide enough power for signals, monitoring sensors and It is very important to recharge the battery of the electric car. This means, the current prototype is a pioneering design of future designs of the same pedal harvester. This research opens a new area of research and invites researchers and engineers to work on it.

References

[1] VARAIYA, P.P.: Smart cars on smart roads: problems of control, *IEEE Transactions on Automatic Control*, Vol. 38, No. 2, pp. 195-207, 1991.

[2] MALIK, J., WEBER, J., LUONG, Q.-T., KOLLER, D.: *Smart cars and smart roads*, Proceedings of the British Machine Vision Conference, Birmingham, UK, pp. 367-382, 1995. http://dx.doi.org/10.5244/C.9.37

[3] KARPIRISKI, M., SENART, A., CAHILL, V.: *Sensor networks for smart roads*, Fourth Annual IEEE International Conference on Pervasive Computing and Communications Workshops (PERCOMW'06), Pisa, Italy, pp. 5-310, 2006. http://dx.doi.org/10.1109/PERCOMW.2006.123

[4] ALWAFAIE, M.A., KOVACS, B.: The mechanism parts of mechanical motion rectifier to produce energy from third pedal in automotive, *Acta Technologia*, Vol. 9, No. 2, pp. 73-77, 2023. https://doi.org/10.22306/atec.v9i2.174

[5] TANG, X., ZUO, L.: Vibration energy harvesting from random force and motion excitations, *Smart Materials and Structures*, Vol. 21, No. 7, pp. 1-9, 2012. http://dx.doi.org/10.1088/0964-1726/21/7/075025

[6] LI, Z., ZUO, L., LUHRS, G., LIN, L., QIN, Y.: Electromagnetic Energy-Harvesting Shock Absorbers: Design, Modeling, and Road Tests, *IEEE Transactions on Vehicular Technology*, Vol. 62, No. 3, pp. 1065-1074, 2013. http://dx.doi.org/10.1109/TVT.2012.2229308

[7] SARMA, B.S., JYOTHI, V., SUDHIR, D.: Design of Power Generation Unit Using Roller Mechanism, *IOSR Journal of Electrical and Electronics Engineering*, Vol. 9, No. 3, pp. 55-60, 2014.

[8] HILL, D., AGARWAL, A., TONG, N.: Assessment of piezoelectric materials for roadway energy harvesting, Cost of Energy and Demonstration Roadmap, Final project report, [Online], Available: http://pop.h-cdn.co/assets/cm/15/06/54d152f0cee9f_-_CEC-500-2013-007.pdf [20 Feb 2024], 2014.

[9] XIONG, Q., QIN, B., LI, X., ZUO, L.: *A Rule-Based Damping Control of MMR-Based Energy-Harvesting Vehicle Suspension*, 2020 American Control Conference (ACC), Denver, CO, USA, pp. 2262-2267, 2020. http://dx.doi.org/10.23919/ACC45564.2020.9147421

[10] WANG, L., TODARIA, P., PANDEY, A., O'CONNOR, J., CHERNOW, B., ZUO, L.: An electromagnetic speed bump energy harvester and its interactions with vehicles, *IEEE/ASME Transactions on Mechatronics*, Vol. 21, No. 4, pp. 1985-1994, 2016. http://dx.doi.org/10.1109/TMECH.2016.2546179

[11] TODARIA, P., WANG, L., PANDEY, A., O'CONNOR, J., MCAVOY, D., HARRIGAN, T., CHERNOW, B., ZUO, L.: *Design, modeling and test of a novel speed bump energy harvester*, In: Proceedings SPIE 9435, Sensors and Smart Structures Technologies for Civil, Mechanical, and Aerospace Systems 2015, Vol. 9435, pp. 38-51, 2015. https://doi.org/10.1117/12.2084371

[12] LI, Z., ZUO, L., KUANG, J., LUHRS, G.: Energy-harvesting shock absorber with a mechanical motion rectifier, *Smart Materials and Structures*, Vol. 22, No. 2, pp. 1-10, 2012. https://doi.org/10.1088/0964-1726/22/2/025008

[13] WANG, L., PARK, J., ZHOU, W., BAN, J., ZUO, L.: On-Road Energy Harvesting From Running Vehicles, [Online], Available: https://rosap.ntl.bts.gov/view/dot/31201/dot_31201_DS1.pdf [20 Feb 2024], 2014.

[14] SALMAN, W., QI, L., ZHU, X., PAN, H., ZHANG, X., BANO, S., ZHANG, Z., YUAN, Y.: A high-efficiency energy regenerative shock absorber using helical gears for powering low-wattage electrical device of electric vehicles, *Energy*, Vol. 159, No. September, pp. 361-372, 2018. https://doi.org/10.1016/j.energy.2018.06.152

[15] TODARIA, P.: *Design, Modelling, and Test of an Electromagnetic Speed Bump Energy Harvester*, Virginia Polytechnic Institute and State University, Blacksburg, Virginia, 2016.

[16] AZAM, A., AHMED, A., HAYAT, N., ALI, S., KHAN, A.S., MURTAZA, G., ASLAM, T.: Design, fabrication, modelling and analyses of a movable speed bump-based mechanical energy harvester (MEH) for application on road, *Energy*, Vol. 214, No. January, p. 118894, 2021.

[17] ALI, A., AHMED, A., ALI, M., AZAM, A., WU, X., ZHANG, Z., YUAN, Y.: A review of energy harvesting from regenerative shock absorber from 2000 to 2021: advancements, emerging applications, and technical challenges, *Environmental Science and Pollution Research*, Vol. 30, No. 3, pp. 5371-5406, 2023.

Review process
Single-blind peer review process.

Acta Tecnología - International Scientific Journal about Technologies
Volume: 10 2024 Issue: 2 Pages: 65-71 ISSN 2453-675X

https://doi.org/10.22306/atec.v10i2.201 Received: 09 May. 2024; Revised: 26 June 2024; Accepted: 28 June 2024

Comparison of mechanical properties polyamide materials produced by different additive technologies

Miroslav Kohan
Technical University of Kosice, Faculty of Mechanical Engineering, Department of Biomedical Engineering and Measurement, Letna 1/9, 042 00 Kosice, Slovak Republic, EU, miroslav.kohan@tuke.sk (corresponding author)
Viktoria Rajtukova
Technical University of Kosice, Faculty of Mechanical Engineering, Department of Biomedical Engineering and Measurement, Letna 1/9, 042 00 Kosice, Slovak Republic, EU, viktoria.rajtukova@tuke.sk
Tomas Balint
Technical University of Kosice, Faculty of Mechanical Engineering, Department of Biomedical Engineering and Measurement, Letna 1/9, 042 00 Kosice, Slovak Republic, EU, tomas.balint@tuke.sk
Jozef Zivcak
Technical University of Kosice, Faculty of Mechanical Engineering, Department of Biomedical Engineering and Measurement, Letna 1/9, 042 00 Kosice, Slovak Republic, EU, jozef.zivcak@tuke.sk
Radovan Hudak
Technical University of Kosice, Faculty of Mechanical Engineering, Department of Biomedical Engineering and Measurement, Letna 1/9, 042 00 Kosice, Slovak Republic, EU, radovan.hudak@tuke.sk

Keywords: SLS Technology, MJF Technology, PA, mechanical properties, orientation.
Abstract: Additive technology provides several advantages compared to traditional production methods, such as creation of complex geometric shapes with less material consumption. However, the setting of the 3D printing process as well as the positioning of the printed object has an impact on the mechanical properties of the material used. The aim of this study was to compare the mechanical properties of polyamide (PA) material as well as the influence of the orientation of printed objects when using SLS and MJF technology. The SLS technology used the P 396 device (EOS, Germany). An HP Jet Fusion 5200 (HP, USA) was used for MJF technology. In both cases, PA was used to creating experimental samples for mechanical testing. The orientation of the printed samples was 0°, 45° and 90° to the base platform of the 3D printer. The results show by comparing SLS and MJF technologies highest mechanical properties for MJF technology when the position samples were at 90° to the basic platform of 3D printer. Conversely, the lowest mechanical properties were recorded for samples that were positioned at a 45° angle to the base platform of the 3D printer using SLS technology.

1 Introduction

Polyamide (PA) is considered a thermoplastic polymer characterized by low density and good thermal stability. PA material is characterized by good properties such as impact, wear against mechanical forces as well as proportional elongation [1]. However, in general, PA material can be divided into several subgroups (e.g. PA46, PA66, PA12 and PA6) [2]. The designation of the subgroups of the PA material refers to the molecular structure that affects the mechanical properties. The subgroup of materials PA 6 represents harder and tougher materials, while PA 12, on the other hand, represents more flexible and pliable materials. However, the melting temperature of the entire group of these materials represents a temperature range of 220°C to 260°C [3].

Due to the different types of polyamides, the scientific community also studies these materials in terms of mechanical properties. One of them is the study by Hofland et al. [4] where they investigated the parameters of 3D printing of SLS technology on the mechanical properties of printed parts of PA12 material. Among the parameters investigated during the production of samples for mechanical testing were preheating temperature, laser power, scanning distance, scanning speed, layer thickness and orientation of the printed object. The results of mechanical testing for the selected settings of the 3D printing process confirmed that the thickness parameter of the applied layer has the greatest influence on the mechanical properties. The orientation of the printed samples (horizontal = 0°; vertical = 90°) with the same parameters of the 3D printing process were also analysed, while different mechanical properties of the PA material were also recorded in this aspect. A similar study called the effect of printing orientation on the tensile strength of PA12 samples obtained by SLS is described by Jevtic et al. [5]. The results of the study describe that samples oriented vertically during the 3D printing process have a higher modulus of elasticity. The authors also hypothesize that the sintering process is more efficient for samples oriented in a vertical position due to a more uniform trajectory of the laser beam than for samples that were oriented horizontally to the base platform of the 3D printer.

Additive technology, also known as 3D printing, is increasingly entering various fields such as automotive

manufacturing [6-8], aerospace industry [9-11], prototyping [12-14], medicine [15-17] or pharmacology [18]. Additive technology currently plays an important role in prototype design. However, it is necessary to realize what is expected from the manufactured prototype and therefore it is important to choose the appropriate type of additive technology during the production of the prototype. Currently, Selective Laser Sintering (SLS) and Multi Jet Fusion (MJF) is often used in the production of prototypes but also in serial production [19]. SLS technology belongs to the general group of additive technology called Laser Powder Bed Fusion (LPBF), which uses a laser to melt plastic grains that have been applied to a platform. Subsequently, the platform is moved lower in the z axis, a new layer of powder material is applied and the laser sinters the material in the required places. This process is repeated until the entire 3D object is created. Selective laser sintering is very popular in the field of plastic 3D printing due to its substantial advantages, such as design freedom, high productivity and low part cost. Unlike some other 3D printing technologies, such as Stereolithography (SLA) or Fused filament fabrication (FFF), SLS and MJF technology does not require any support structures. This enables the creation of very complex patterns [20-22].

The 3D printing process of MJF technology can be divided into the following points. The printer's dispenser applies a thin layer of powder material to the platform. Then the ink head applies a liquid agent, which comes in two variants. The first type (fixing) connects the individual layers together and the second type (detailing) is used to define the exact surface dimensions of the printed parts. A heating unit is used to harden the individual layers, which is activated after the agent is applied. The advantage of this technology is the use of bulk material, which eliminates the creation of supporting structures, which results in the creation of complex structures (like SLS technology). Part of the production process is also the so-called postprocessing, where excess material is removed. Used material can be reused when mixing with new material in 20/80 (new material / used material). MJF technology based on its principles is used for serial production of printed parts as well as prototyping. By comparing SLS and MJF technology, it can be said that these technologies are similar in terms of the input materials used, but SLS technology uses sintering to join individual layers, while MJF uses reagents and heating to join individual layers.

There are several scientific studies comparing SLS and MJF technology. In a study by Rosso et al. [23] investigated an in-depth comparison of PA12 parts produced by SLS and MJF technology. The study analyzed the material properties of PA12 printed samples from PA12 as well as the mechanical behavior of selected structures in tensile and fatigue tests. The results of mechanical tests showed that samples produced by SLS technology appear to be stiffer with lower plastic deformation compared to samples produced by MJF technology. Fatigue tests represent a higher dispersion for samples produced with MJF technology and an increase in fatigue life. A similar study by Xu et. al. [24], which was devoted to the comparison of the SLS and MJF technology processes while evaluating the morphology, thermal and mechanical properties of PA12 parts. The results of the study showed that the PA12 material in powder form using these technologies had approximately elliptical shapes of similar size. In the case of the produced samples, the surface roughness of the samples produced by the MJF technology showed better values than that of the samples produced by the SLS technology. During the printing process with the function of immediate laser cutting, the degree of melting of particles with SLS technology was higher than with MJF technology. The results of the mechanical properties of the printed samples were better with the SLS technology. In terms of time, the printing speed with MJF technology was 10 times higher than with SLS technology.

The aim of the presented work is to compare the mechanical properties of samples produced by two different additive technologies. A difference is assumed between the positions of the samples as well as between the production technologies.

2 Material and methodology

2.1 Material characteristics

To compare the individual additive technologies in terms of the mechanical properties of the PA12 material, the material PA 2200 (EOS, Germany) based on PA12 using SLS technology was chosen. In the second case, the MJF technology was chosen using the input material PA12 under the trade name HP 3D HR PA12 (HP, Germany). The selection of materials was chosen based on the technologies used, which use only certified materials from 3D printer manufacturers. The technical specification of the materials is described in Table 1.

Table 1 Specification of materials

	PA2200	**PA12**
Density [g/cm^3]	0.93	1.02
Average grain size [µm]	65	60
Melting point [°C]	176	187
Glass transition [°C]	~ 55	~ 50

2.2 Samples production procedure

The design of the experimental samples was implemented in SolidWorks 2019 software (Dassault Systèmes, USA). The design of the proposed sample was based on the valid standard for mechanical testing STN EN SIO 527-2: 2012. Individual variations of the proposed sample are described in Figure 1.

Comparison of mechanical properties polyamide materials produced by different additive technologies

Miroslav Kohan, Viktoria Rajtukova, Tomas Balint, Jozef Zivcak, Radovan Hudak

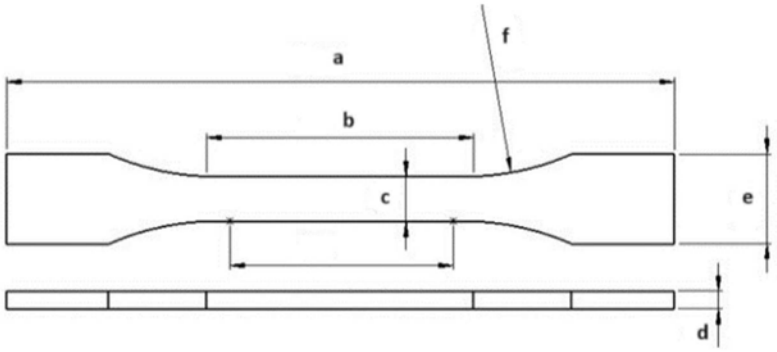

Figure 1 Dimensions of test samples (a:Total length 150 mm; b: Lenght of the narrow parallel part 60 mm; c: Width of the narrow part 10 mm; d: thickness 4 mm; e: Width at the end 20 mm; f: radius 60 mm)

The samples were divided into 3 groups according to the positioning during the 3D printing process (Figure 2). The difference in orientation for individual groups was as follows:

- Group A: position of samples at 0 angle (on the mat), 20 pieces of samples.
- Group B: position of the samples at a 45° angle to the horizontal axis, 20 pieces of samples.
- Group C: position of the samples at a 90° angle to the horizontal axis, 20 pieces of samples.

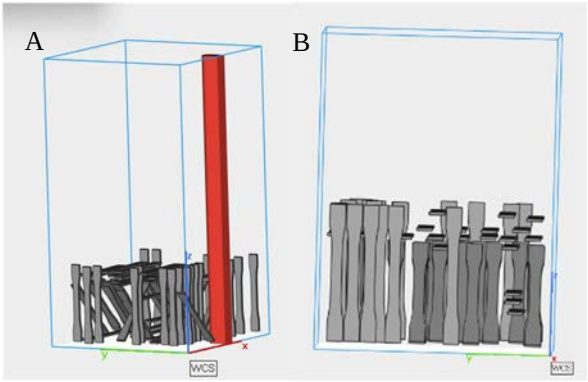

Figure 2 Preparation of samples for EOS and for HP (A: SLS Technology; B: MJF Technology)

The production of experimental samples was carried out using two technologies. One of them was the SLS technology behind the EOS P396 device (EOS, Germany). In the second case, MJF technology was chosen for the HP Jet Fusion 5200 device (HP, USA). In both cases of the chosen technology, PA12 material was used. The set parameters of 3D printing are described in Table 2.

Table 2 Parameters of 3D printing process for SLS and MJF technologies

	EOS P396	**HP 5200**
Building speed [m/s]	6	0.014
Layer thickness [mm]	0.12	0.08
Sintering energy source	Heating lamp	Energy
Powder mixture	50:50	20 fresh:80 recycled
Powder melting point [°C]	187	176

2.3 Mechanical testing

Mechanical tensile testing was performed on 120 samples (Figure 3). The samples were divided into 3 test groups (Group A: sample position at 0°; Group B: sample position at 45°; Group C: sample position at 90°). An Inspekt Table (Hegewald & Peschke, Nossen, Germany) with a measuring range of 5 kN was used for mechanical testing. The tensile testing speed was set at 2 mm/min. The relative elongation was measured on RTSS extensometer (Limess, Germany) while the initial length was 50 mm. The distance between the clamping jaws was 115 mm.

Figure 3 Produced samples for mechanical testing (A: samples produced by SLS Technology; B: samples produced by MJF Technology)

3 Results and discussion

3.1 Comparison of mechanical properties of PA material based on sample position

The investigated parameters of the mechanical properties of PA material based on the positioning of the

sample were ultimate strength (Rm) and Young's modulus of elasticity (E). In Figure 4 individual groups of samples are graphically represented and compared.

When SLS technology was used, the average Rm value for sample group A was 43.52 ± 1.65 MPa, for sample group B at 40.86 ± 0.57 MPa and for sample group C at 42.63 ± 0. 47 MPa. Comparing the average values of the Rm parameter, differences were found at the level of 2.66 MPa (group A versus group B). By comparing the same parameter between sample groups A and C, differences were detected at the level of 0.89 MPa. From this, it can be concluded that the positioning of the experimental samples at a zero angle (on the base platform of the 3D printer) shows the best mechanical properties of the samples made of PA material. Conversely, the lowest Rm was recorded for samples that were positioned at a 45° angle during the 3D printing process. The analysis of parameter E using SLS technology showed average values for sample group A at a value of 1464 ± 78.4 MPa, for sample group B at a value of 1425.49 ± 44.41 MPa and for sample group C at a value of 1465.85 ± 34, 97 MPa. By comparing the average values of the parameter E, differences were recorded at the level of 38.51 MPa in favor of the samples that were positioned at a zero angle to the base platform of the 3D printer. When comparing groups, A and C, these differences in average values were recorded at the level of 40.36 MPa.

When using the MJF technology, specifically for the parameter Rm, the average values were recorded for the sample group A at a value of 42.66 ± 1.67 MPa, for group B the value was 42.67 ± 1.63 MPa and for group C the value was 45.25 ± 1.1 MPa. In this case, the best mechanical properties of the samples were achieved with group C (position of the samples 90° to the basic platform of the 3D printer). The differences in mean Rm values were 2.59 MPa (group C versus A). A similar result was recorded when comparing the average values between sample groups C and B (2.58 MPa). The analysis of parameter E using MJF technology showed average values for sample group A at a value 1453.2 ± 43.35 MPa, for samples group B at a value of 1523.03 ± 37.34 MPa above for sample group C at a value of 1559.1 ± 99.8 MPa. The highest differences of these average values were observed between sample groups A and C (105.9 MPa). It is evident from the results that the position of the experimental samples below 90° to the basic platform of the 3D printer shows the highest values of the E parameter.

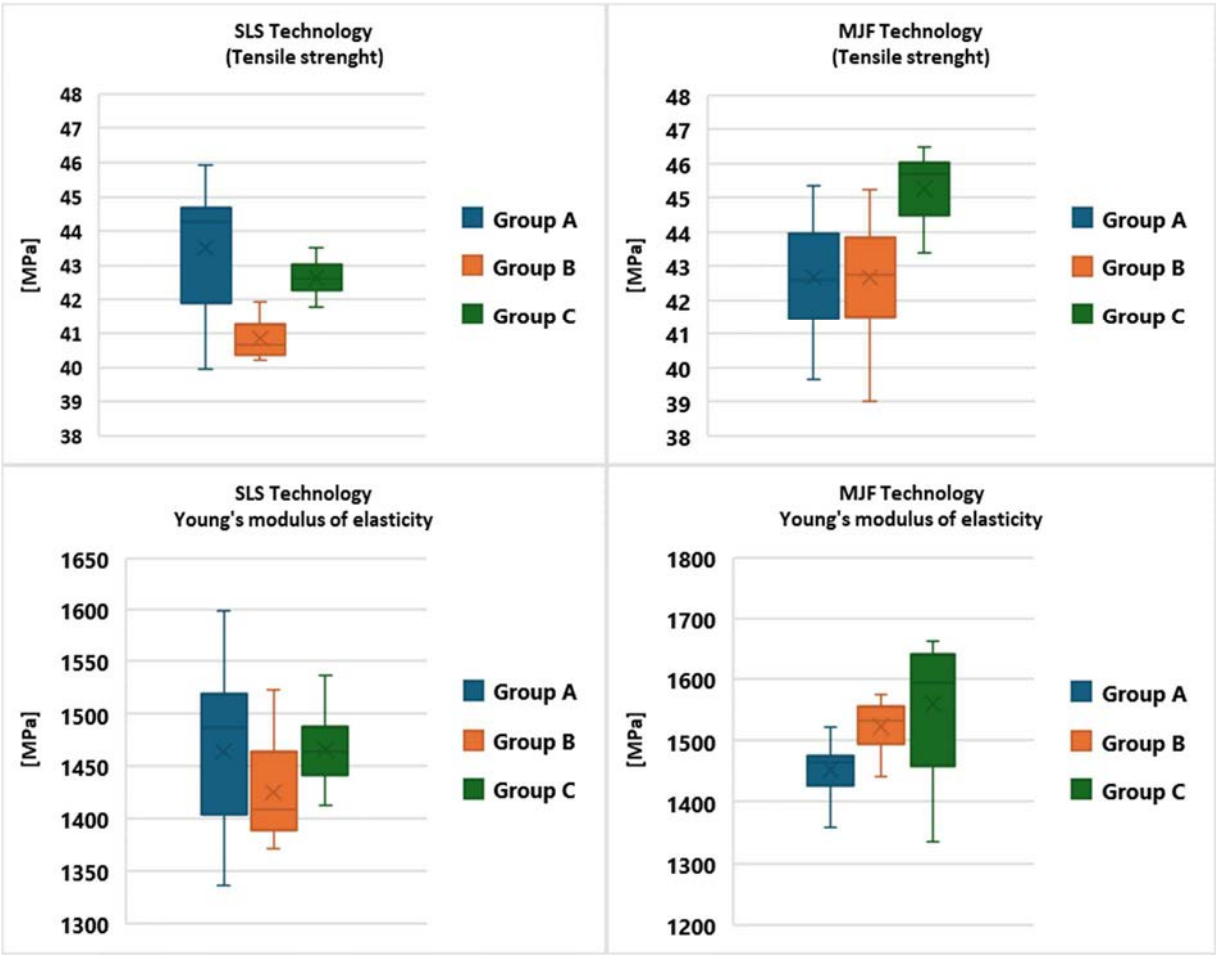

Figure 4 Comparison of mechanical properties of experimental samples at different positions during the 3D printing process

3.2 Comparison of mechanical properties of PA material based on production technology

The comparison of the mechanical properties of the PA material based on the production technology was performed on the parameters Rm and E. In Figure 5 are a graphic representation and comparison of individual production technologies.

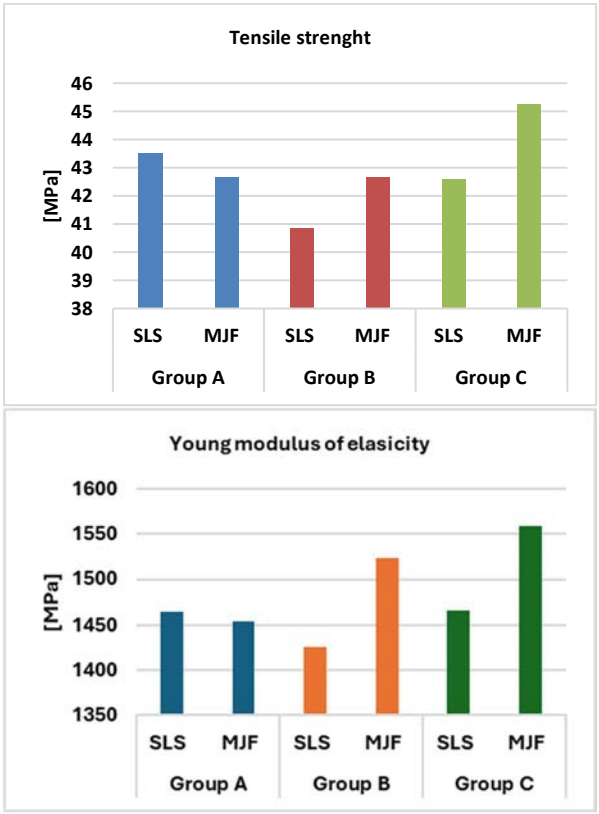

Figure 5 Comparison of mechanical properties of experimental samples based on production technology

Comparing SLS and MJF technologies in terms of Rm, certain differences were noted, while in sample group A this difference was at a value of 0.86 MPa, in sample group B at a value of 1.81 MPa and in sample group C at the level of 2.62 MPa. By comparing the average values of the Rm parameter, it can be concluded that the production SLS technology has better mechanical properties if the printed sample was positioned at a zero angle to the basic platform of the 3D printer. However, for the remaining sample positions (45° and 90°), the Rm values were higher for the MJF technology. Comparing the technologies when examining the parameter E, similar results were achieved, but with higher levels of difference. By comparing the average values of the parameter E, it can be concluded that the production SLS technology has better mechanical properties for samples that were produced at a zero angle to the basic platform of the 3D printer (difference at the level of 10.8 MPa). However, for samples that were printed at 45° and 90° angles to the base platform, these values of the parameter E were significantly lower compared to the MJF technology. The difference in this case was at the level of 97.54 MPa for group B and 93.25 MPa for group C samples.

4 Conclusion

In this study, we used SLS and MJF technology to investigate the mechanical properties at different positions of printed objects on the ideal position in terms of parameters Rm and E. The results showed that when comparing SLS and MJF technologies, the highest mechanical properties were recorded when MJF technology was used while positioning the sample at a 90° angle to the base platform of the 3D printer. Conversely, the lowest mechanical properties were recorded for samples that were positioned at a 45° angle to the base platform of the 3D printer using SLS technology. The study also demonstrated that additive technology and its correct setting and position of printed objects is possible to regulate the mechanical properties of manufactured parts.

Acknowledgement

This publication is the result of the project implementation Research and development of intelligent traumatological external fixation systems manufactured by digitalisation methods and additive manufacturing technology (Acronym: SMARTfix), ITMS2014+: 313011BWQ1 supported by the Operational Programme Integrated Infrastructure funded by the European Regional Development Fund. This research was supported by project KEGA 050TUKE-4/2022 Additive manufacturing in medicine - creation of multimedia material and tools to support teaching in biomedical engineering. This research was supported by project VEGA 1/0599/22 Design and biomechanical analysis of personalized instruments for arthroscopic applications.

References

[1] UNAL, H., MIMAROGLU, A.: Friction and wear performance of polyamide 6 and graphite and wax polyamide 6 composites under dry sliding conditions, *Wear*, Vol. 289, No. June, pp. 132-137, 2012. https://doi.org/10.1016/j.wear.2012.04.004

[2] GILBERT, M.: *Aliphatic Polyamides*, Brydson's Plastics Materials, Elsevier, pp. 487-511, 2017. https://doi.org/10.1016/B978-0-323-35824-8.00018-9

[3] COUSSENS, B., RULKENS, R.: Effect of amide distribution in polyamide isomers on their melting points, *Journal of Applied Polymer Science*, Vol. 135, No. 9, 2018. https://doi.org/10.1002/app.45837

[4] HOFLAND, E.C., BARAN, I., WISMEIJER, D.A.: Correlation of Process Parameters with Mechanical Properties of Laser Sintered PA12 Parts, *Advances in Materials Science and Engineering*, Vol. 2017, pp. 1-11, 2017. https://doi.org/10.1155/2017/4953173

[5] JEVTIĆ, I., GOLUBOVIĆ, Z., MLADENOVIĆ, G., BERTO, F., SEDMAK, A., MILOVANOVIĆ, A., MILOŠEVIĆ, M.: Printing orientation influence on

tensile strength of PA12 specimens obtained by SLS, *Journal of Mechanical Science and Technology*, Vol. 37, No. 11, pp. 5549-5554, 2023. https://doi.org/10.1007/s12206-023-2306-4

[6] VASCO, J.C.: *Chapter 16 - Additive manufacturing for the automotive industry*, Editor(s): Juan Pou, Antonio Riveiro, J. Paulo Davim, In: Handbooks in Additive Manufacturing, Additive Manufacturing, Elsevier, pp. 505-530, 2021. https://doi.org/10.1016/B978-0-12-818411-0.00010-0

[7] MOHANAVEL, V., ASHRAFF ALI, K.S., RANGANATHAN, K.: The roles and applications of additive manufacturing in the aerospace and automobile sector, *materialstoday: Proceedings*, Vol. 47, part 1, pp. 405-409, 2021. https://doi.org/10.1016/j.matpr.2021.04.596

[8] LUNIYA, T., CHIMATA, G.: *Extending the Life of Classic Cars, the Additive Manufacturing Way*, In: Volume 2A: Advanced Manufacturing, American Society of Mechanical Engineers, 2021. https://doi.org/10.1115/IMECE2021-70355

[9] NAJMON, J.C., RAEISI, S., TOVAR, A.: *Review of additive manufacturing technologies and applications in the aerospace industry*, In: Additive Manufacturing for the Aerospace Industry, Elsevier, pp. 7-31, 2019. https://doi.org/10.1016/B978-0-12-814062-8.00002-9

[10] KALENDER, M., KILIC, S.E., ERSOY, S., BOZKURT, Y., SALMAN, S.: *Additive Manufacturing and 3D Printer Technology in Aerospace Industry*, In: 9th International Conference on Recent Advances in Space Technologies (RAST), IEEE, 2019, pp. 689-694, 2019. https://doi.org/10.1109/RAST.2019.8767881

[11] FU, X.X., LIN, Y.X., YUE, X.J., XUNMA, HUR, B., ZHENG YUE, X.: *A Review of Additive Manufacturing (3D Printing) in Aerospace: Technology, Materials, Applications, and Challenges*, In: TANG, Dalai, ZHONG, Joni a ZHOU, Dalin (ed.), Mobile Wireless Middleware, Operating Systems and Applications, EAI/Springer Innovations in Communication and Computing, Cham: Springer International Publishing, 2022, pp. 73-98, 2022. https://doi.org/10.1007/978-3-030-98671-1_6

[12] BOCHNIA, J., KOZIOR, T.: Methods of Prototyping Process Using Modern Additive Technologies, *Solid State Phenomena*, Vol. 223, pp. 199-208, 2014. https://doi.org/10.4028/www.scientific.net/SSP.223.199

[13] ROBINSON, D.K.R., LAGNAU, A., BOON, W. P.C.: Innovation pathways in additive manufacturing: Methods for tracing emerging and branching paths from rapid prototyping to alternative applications, *Technological Forecasting and Social Change*, Vol. 146, pp. 733-750, 2019. https://doi.org/10.1016/j.techfore.2018.07.012

[14] GIBSON, I., ROSEN, D., STUCKER, B.: *Additive Manufacturing Technologies*, New York, Springer New York, 2015. https://doi.org/10.1007/978-1-4939-2113-3

[15] KUMAR, A., KUMAR, D., FAISAL, N., SHARMA, A., KUMAR ANSU, A., GOYAL, A., SAXENA, K.K., PRAKASH, C., KUMAR, D.: Application of 3D printing technology for medical implants: a state-of-the-art review, *Advances in Materials and Processing Technologies*, Vol. 10, No. 2, pp. 357-372, 2023. https://doi.org/10.1080/2374068X.2023.2193788

[16] ARIF, Z.U., KHALID, M.Y., NOROOZI, R., HOSSAIN, M. et al. Additive manufacturing of sustainable biomaterials for biomedical applications, *Asian Journal of Pharmaceutical Sciences*, Vol. 18, No. 3, pp. 1-36, 2023. https://doi.org/10.1016/j.ajps.2023.100812

[17] BAHATI, D., BRICHA, M., EL MABROUK, K.: Vat Photopolymerization Additive Manufacturing Technology for Bone Tissue Engineering Applications, *Advanced Engineering Materials*, Vol. 25, No. 1, 2023. https://doi.org/10.1002/adem.202200859

[18] MUHINDO, D., ELKANAYATI, R., SRINIVASAN, P., REPKA, M.A., ASHOUR, E.A.: Recent Advances in the Applications of Additive Manufacturing (3D Printing) in Drug Delivery: A Comprehensive Review, *AAPS PharmSciTech*, Vol. 24, No. 2, pp. 1-22, 2023. https://doi.org/10.1208/s12249-023-02524-9

[19] LIPSON, H., KURMAN, M.: *Fabricated: the new world of 3D printing; [the promise and peril of a machine that can make (almost) anything]*, Indianapolis, Wiley, 2013.

[20] RAZAVIYE, M.K., TAFTI, R.A., KHAJEHMOHAMMADI, M.: An investigation on mechanical properties of PA12 parts produced by a SLS 3D printer: An experimental approach, *CIRP Journal of Manufacturing Science and Technology*, Vol. 38, No. August, pp. 760-768, 2022. https://doi.org/10.1016/j.cirpj.2022.06.016

[21] CHAROO, N.A., BARAKH ALI, S.F., MOHAMED, E.M., KUTTOLAMADOM, M.A., OZKAN, T., KHAN, M.A., RAHMAN, Z.: Selective laser sintering 3D printing – an overview of the technology and pharmaceutical applications, *Drug Development and Industrial Pharmacy*, Vol. 46, No. 6, pp. 869-877, 2020. https://doi.org/10.1080/03639045.2020.1764027

[22] KUSHWAHA, A.K., RAHMAN, M.H., SLATER, E., PATEL, R., EVANGELISTA, CH., AUSTIN, E., TOMPKINS, E., MCCARROLL, A., RAJAK, D.K., MENEZES, P.L.: *Powder bed fusion–based additive manufacturing: SLS, SLM, SHS, and DMLS*, In: Tribology of Additively Manufactured Materials, Elsevier, pp. 1-37, 2022.

https://doi.org/10.1016/B978-0-12-821328-5.00001-9

[23] ROSSO, S., MENEGHELLO, R., BIASETTO, L., GRIGOLATO, L., CONCHERI, G., SAVIO, G.: In-depth comparison of polyamide 12 parts manufactured by Multi Jet Fusion and Selective Laser Sintering, *Additive Manufacturing*, Vol. 36, pp. 1-13, 2020. https://doi.org/10.1016/j.addma.2020.101713

[24] XU, Z., WANG, Y., WU, D., ANANTH, K.P., BAI, J.: The process and performance comparison of polyamide 12 manufactured by multi jet fusion and selective laser sintering, *Journal of Manufacturing Processes*, Vol. 47, No. November, pp. 419-426, 2019. https://doi.org/10.1016/j.jmapro.2019.07.014

Review process
Single-blind peer review process.

Acta Tecnología - International Scientific Journal about Technologies
Volume: 10 2024 Issue: 2 Pages: 73-79 ISSN 2453-675X

Development of a robotic handwriting assistant for children with movement disorder
Ismael Breton, Alexandre Campeau-Lecours

https://doi.org/10.22306/atec.v10i2.203 *Received: 12 June 2024; Revised: 21 June 2024; Accepted: 27 June 2024*

Development of a robotic handwriting assistant for children with movement disorder

Ismael Breton
Université Laval, Department of Mechanical Engineering, 1065 Av. De la Médecine, Quebec City, QC, Canada, G1V 0A6, ismael.breton.1@ulaval.ca (corresponding author)
Alexandre Campeau-Lecours
Université Laval, Department of Mechanical Engineering, 1065 Av. De la Médecine, Quebec City, QC, Canada, G1V 0A6, alexandre.campeau-lecours@gmc.ulaval.ca

Keywords: mechatronics, developmental coordination disorder, assistive technologies, robotics, handwriting.
Abstract: Developmental coordination disorder (DCD) impairs motor skills in children, particularly handwriting, which is a significant part of school activities and personal development. Current robotic assistants often lack a fully physical interaction or tangible result, thereby limiting their effectiveness in coordination development similar to handwriting. To address this gap, a robotic assistant capable of physical input and output could enhance development. This paper presents the development of a robotic handwriting assistant to aid children with DCD. The prototype is a planar robot controlled via a joystick capable of covering an 8.5" by 11" paper sheet. The paper provides insight into the causal real-world context of the prototype's development and discusses the designs considerations, the conception and the control. It concludes with intial results and the future for the project.

1 Introduction

Developmental Coordination Disorder (DCD) is prevalent among children aged 5 to 11, affecting approximately 8% of Canadian children. This condition, characterized by impaired motor skills, can stem from various neurological and neuromuscular disorders, including cerebral palsy, ataxia and muscular dystrophy [1]. Furthermore, DCD and attention-deficit/hyperactivity disorder (ADHD) comorbidity is quite frequent [2]. Consequentially, children with DCD often struggle to participate in physical activities at the same level as their peers, exhibiting slower task completion [3]. Poor coordination can result in a more sedentary lifestyle and increased fatigue due to inefficient movement, thereby negatively impacting the daily lives of both children and adults living with DCD [4].

Handwriting, a common school skill, poses significant challenges for children with DCD. This graphomotor skill demands various capacities, including hand function, perception, and motor control, which individuals diagnosed with DCD often lack [5]. Consequently, it becomes a source of frustration as it hampers their ability to express their creativity, limits their learning potential and diminishes their interest in handwriting. In a common scenario at school, such as a math class, handwriting is mostly required to complete problems. Children with DCD use more time and energy just to concentrate on the writing. Therefore, it leaves them with less time to complete the problem. It creates a severe imbalance between the time used to concentrate on the step and the times used to concentrate on writing.

Using computers and tablets for writing and drawing is a contemporary approach that offers accessibility and simplicity to compensate for the effects of DCD. However, research indicates that the sensory information inherent in handwriting fosters stronger memory retention compared to computer typing [6]. Moreover, students tend to reframe their notes in their personal language when handwriting, whereas computer typing tends to enforce a more rigid note-taking approach [7, 8]. In summary, for the purposes of adaptation and coordination enhancement, a physical input and output system is superior to computers, considering the benefits of memory improvement and the freedom afforded in notetaking.

Two types of devices can be considered for children with. Firstly, there are mechanical aids to support the correct way of grasping the pen [9,10]. They allow greater handling while writing. Secondly, there are devices that facilitate handwriting tasks for those living with stiffness and mitigate unwanted motion [11]. This project is in the later category.

Previous studies have explored the integration of robotic devices in enhancing children's handwriting skills [12]. One such trial utilized a haptic 6 degrees of freedom (DOFs) robotic system known as the "PHANTOM Omni" [13]. A comparison was made between the performance of children who had prior exposure to the robotic device and those who had not, revealing promising results in motor skill development. However, the substantial cost associated with these tools was noted. As of 2024, the "PHANTOM Omni," now rebranded as the "Geomagic Touch", has a price tag of $3400 USD [14]. Alternatives like the AxiDraw SE/A3 from *Evil Mad Scientist* are available, boasting excellent drawing quality [15]. However, its main use is as a drawing plotter, relying on virtual inputs rather than manual writing, makes it less

suitable. for coordination development. Furthermore, with a price of 1160 euros ($1260 USD), it remains expensive [16].

Handwriting is important for the development of children and robotic systems can play a significant role in providing a writing tool for those living with DCD. In observation of the current technologies in this sector, or lack thereof, there is a potential need for and assistive tool to develop the coordination and the motors skills of children with DCD.

In previous studies, the robotics systems had either virtual input or output, thereby diminishing the benefits in development from an entirely physical system. To maximise the benefits, the robotic assistant should integrate both physical input and output capabilities.

This paper presents the development of a prototype of a robotic handwriting assistant for children with DCD. It begins with the modeling of the robot and the selection of hardware components to ensure the design of a user-friendly system. Subsequently, the focus is on the design and programming steps aimed at maximizing the robot's performance while keeping the system as simple as possible. Finally, the paper addresses the current capabilities of the robot and its future work.

2 Goal and Objective

The project has the following goal: To provide children with movement disorder the ability to perform writing tasks in a way to develop motor skills and express their creativity.

The main objective of this project is to develop a low-cost robot able to move a pen to draw and write. This robot must be directly controlled by the user via a controller and must have a usable workspace big enough to cover an 8.5” by 11” sheet of paper.

3 Methodology

The robotic handwriting assistant is a parallel robot with two degrees of freedom (DoFs). Its design is shown in Figure 1. It is driven by two stepper motor in a coaxial configuration (one atop the other). The end effector is a servomotor actuated mechanism to raise and lower the pen.

The user can control the robot with a single joystick equipped with a button. An 8.5” by 11” sheet of paper can be set up on the ABS (plastic) plate. When powered, the user can control the cartesian speed of the pen with the joystick. All the electronics, apart from the motors and the joystick, are enclosed in a box beside the motors. The system is installed on a veneer base.

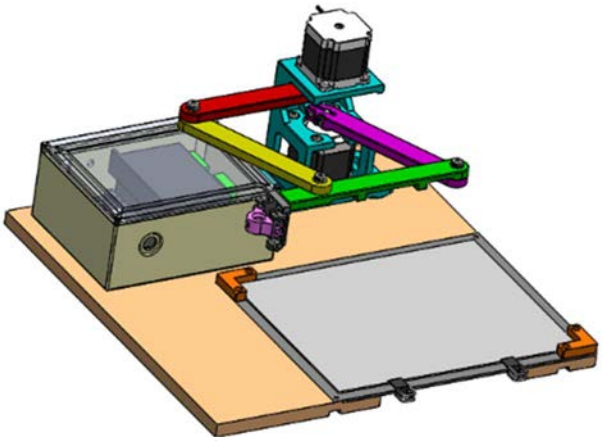

Figure 1 CAD model of the robotic handwriting assistant

The development of the prototype is divided into four iterative parts: I) Selecting the right motor technology for the actuation, II) Selecting a geometrical architecture that suffice the workspace requirements, III) Conception and assembly and IV) Control of the robot.

3.1 Motor technology

To ensure a good pen line quality, which is defined as a uniform line, two motor technologies have been compared: the servomotor and the stepper motor. The test is as followed: Draw five back and fort lines in an arc pattern and compare the quality of the line. The setup of both motors' testing are shown in Figure 2:

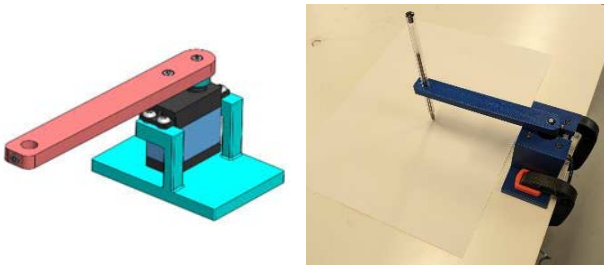

(a) (b)

Figure 2 Assembly of the servomotor (a) and stepper motor (b) test bench to compare the line quality

The tested motors where the model FT6335M from *Feetech* for the servomotor and the model 17HS13 from *StepperOnline* for the stepper motor. The servomotor is position controlled with a discretized trajectory, whereas the stepper motor is speed controlled using a trapezoidal speed profile. During the tests, we observed that the pen line had noticeable vibration with the servomotor. The consensus was that backlash in the motor's gearbox was too great using the standard servo library of *Arduino*. In comparison, the stepper motor proved superior in terms of line quality. In addition, stepper motors have the capability of instant velocity changes at speeds lower than 600RPM, only limited by the maximum speed and torque specified. Therefore, it was decided to use stepper motors for the prototype.

3.2 Architecture and mechanism

The robotic assistant requires an architecture that enables the pen to cover an 8.5" by 11" sheet of paper. The initially proposed architecture shown in Figure 3 (a) is a five-bar linkage mechanism with both motors at different positions. The second architecture shown in Figure 3 (b) is also a five-bar linkage mechanism. However, both motors are now coaxial and all bars, with the exception of the offset length l_2, have the same length l_1. An advantage of this architecture is its modeling. Indeed, due to the equal length of the bars, the system can be kinematically simplified to a two DoFs planar serial robot. Consequently, the control of the system is simpler. As shown in Figure 3 (b), the greyed out bars are redundant in the kinematics. But, they are necessary to transfer the motion of the second motor.

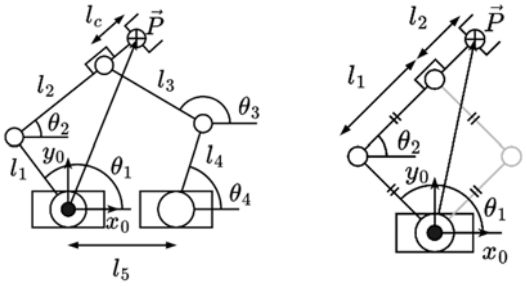

(a) (b)

Figure 3 Standard eccentric five-bar linkage (a) and the chosen five-bar linkage (b). All main bars have the same length of l_1 and the motors are concentric

The parallel architecture is chosen instead of the serial RR (two revolute joints in series) architecture for two reasons. First of all, if the motors were directly connected at the joints, the motor at the second joint would add a significant mass on the arms and cause sagging. Second of all, using a belt system for the second joint would have added multiple mechanical parts and increase the cost of the system. The origin $[x_0, y_0]$ is positioned at the concentric axis of the motors and the cartesian position of the pen is represented as $\vec{P}$. The angle θ_1 is controlled by motor #1 and θ_2 is controlled by the motor #2. As seen in figure Figure 3 (b), the angle θ_2 is also the angle for the second link of the simplified robot geometric (in black).

The system's geometry and a sheet of paper are modeled as shown in Figure 4. Then, using an iterative method, the dimensions of the bars and the position of the sheet in respect of the motors position are selected. Following the analysis, he length l_1 is set at 0.15m and the length l_2 is set at 0.065m.

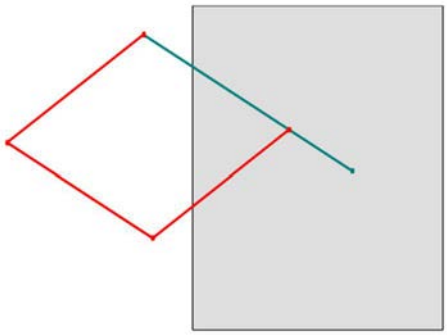

Figure 4 Selection of the bar's dimensions using Solidworks, The red bars all have the same length l_1 and the teal bar has a length $l_1 + l_2$

3.3 Design

3.3.1 Mechanical Hardware

The main mechanical components of the mechanism, be the motor support, bars and pen holder, are 3d printed in PLA. PLA, and fused deposit modeling (FDM) printing, have the advantage of being low cost and quick to manufacture new parts. PLA has sufficient mechanical properties for the robot's requirement. For the joints, shoulder screws are used. They slide in plastic bushings and are screwed in heat inserts. The proximal bars are directly connected to the shaft of both motors.

The pen holder uses a cam, shown in Figure 5 in red, directly connected to a servomotor to move the pen support, shown in purple, vertically. The motion is guided with two pins side-by-side of the cam and springs help to counter the friction and, subsequently, lower the pen.

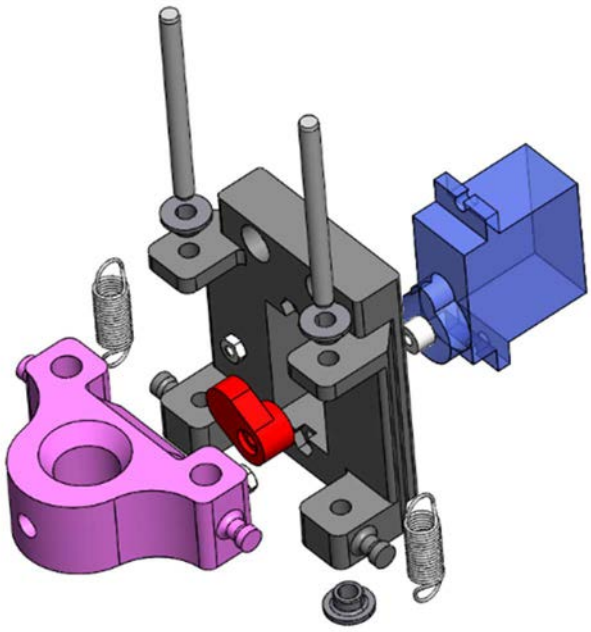

Figure 5 Exploded view of the pen holder

The platform is a veneer base which has been CNC machined, whereas the base for the paper is made of ABS which has been manually machined.

3.3.2 Electrical hardware

The selected motors are the NEMA 23HS56 driven by DM556T motor drives both from *StepperOnline*. These drives offer multiple settings of microstepping, which helps to increase the resolution of the motion. The value for microstepping has been set at 2000 µsteps/rotation.

The model of the servomotor for the pen is the SG90. Its small dimensions and low weight are perfect for the actuator.

The µcontroller is an Arduino Mega 2560. To power all three motors, at least three different fast pulse width modulation (PWM) timers are required. The Arduino Mega 2560 has four 16-bits timers and a good amount of general purpose input/output (GPIO), which makes it suitable for the prototype.

The joystick is a simple dual-axis joystick with spring loaded potentiometers and a single button. These three inputs are sufficient to move the pen and raise/lower it.

3.4 Programming

3.4.1 Model

The mathematic model of the robot arm, using the vector loop method, is represented in scalar values by the equations (1) and (2):

$$x = l_1 \cos\theta_1 + (l_1 + l_2)\cos\theta_2 \quad (1)$$

$$y = l_1 \sin\theta_1 + (l_1 + l_2)\sin\theta_2 \quad (2)$$

These equations are the direct kinematic of the robot. When the equations (1) and (2) are derived in respect to time, it is possible to determine the relationship between cartesian speed and angular speed. This relation is shown in the equation (3):

$$\dot{\vec{P}} = \boldsymbol{J}\dot{\vec{\theta}} \quad (3)$$

where $\boldsymbol{J}$, defined as the Jacobian matrix, has these values:

$$\boldsymbol{J} = \begin{bmatrix} -l_1 \sin\theta_1 & -(l_1 + l_2)\sin\theta_2 \\ l_1 \cos\theta_1 & (l_1 + l_2)\cos\theta_2 \end{bmatrix} \quad (4)$$

3.4.2 Control

The handwriting assistant uses speed control illustrated in the Figure 6. First and foremost, the joystick inputs are read and transformed into a speed value in cartesian space. Subsequently, the inverse Jacobian is used to output the motor's desired angular speed from the cartesian speed. The last step is to transform the angular speed into PWM frequencies. As the speed increases, the frequency is higher. This relationship is linear and based on the motor stepping. At each pulse, the drivers commute. Then, the motors achieve a new step and the angle gets updated in the µcontroller. These angles are used in the inverse Jacobian and the direct kinematic.

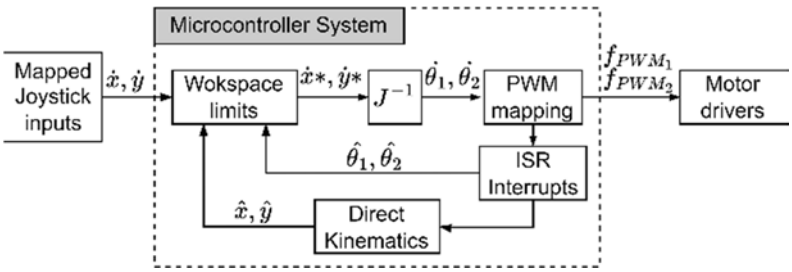

Figure 6 Schematic of the simplified kinematic control

A challenge in the motion control is the change of direction of any motors. The motor drivers require a PWM input and a direction (DIR) input. To assure a stable direction update, the PWM timers are turned off during the change in direction states. Beforehand, a delay of 10 microseconds is added, which is shown in Figure 7. Following the updates, a second delay of 300 microseconds is added. Finally, the PWM timers are turned back on.

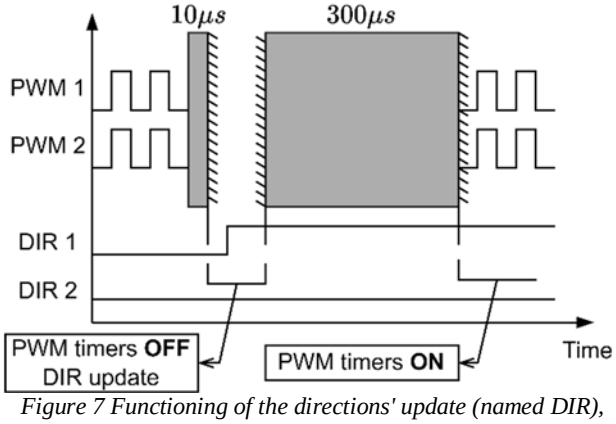

Figure 7 Functioning of the directions' update (named DIR), and control of the PWM timers during this update

3.4.3 Workspace limits

To assure a safe usage of the robot without any collision between the bars and the motor mount and without reaching the geometric limits of the robot, defined as singularity, software limits have been added. The workspace limits are shown in the figure Figure 8. The defined angular limits are a maximum angle of 180° for the first motor ($\theta_{1,MAX}$) and a minimum angle of 0° for the second motor ($\theta_{2,MIN}$). By intuition and physical measurements of the pen position at critical positions of the robots, The minimum radius R_{min} is set at 0.15 meters and the maximum radius R_{max} is set at 0.36 meters.

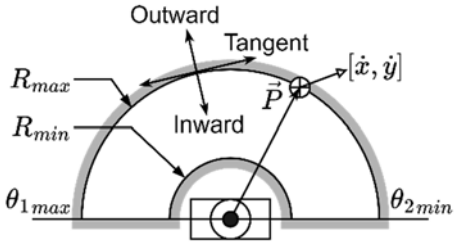

Figure 8 Software limits represented in the physical workspace in front of the actuators

When the robot reaches the radius limits, calculated using the direct kinematic, the orientation of the desired motion ($\dot{x}$ and $\dot{y}$) is compared to the vector comprised of the position ($\hat{x}$ and $\hat{y}$) using the scalar product (SP), which is (5):

$$SP = \hat{x}\dot{x} + \hat{y}\dot{y} \quad (5)$$

The Table 1 explains the program's behaviour based on the scenario:

Table 1 Programmed behavior of the robot based on the workspace limits and desired motion. A desired motion that is allowed (Inward, Outward or Tangent) is represented as "Yes" and a motion that is denied is represented as "No"

Radius Reached	Inward	Outward	Tangent
R_{min}	No	Yes	Yes
R_{max}	Yes	No	Yes

4 Results and discussion

This paper has presented the cycle of development of the prototype robotic handwriting assistant. The first prototype is shown in the Figure 9.

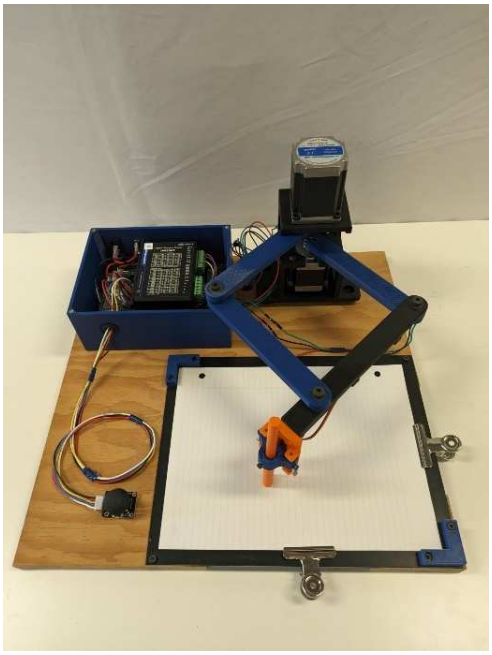

Figure 9 Prototype of the robotic handwriting assistant

4.1 Drawing performance

The performance was evaluated with multiple passes horizontally, vertically and diagonally. Additionally, a circular pattern was tested.

Following the results in the Figure 10, we observe a good quality of the straight lines both horizontally and vertically. During the reverse of directions, the robot performs worse with the vertical lines compared to the horizontal lines. More precisely, the pen moves a little horizontally when changing direction.

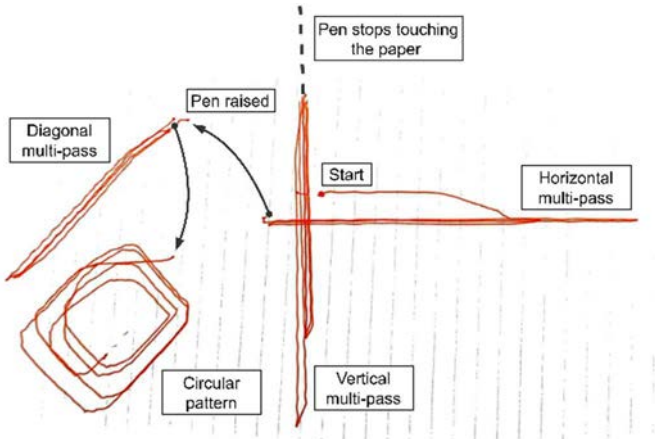

Figure 10 Results of the drawing tests. This includes multiple straight passes in different directions and a circular pattern. The pen is moving at a linear speed of 0.05m/s.

For the diagonal pattern, the pen tends to have regular vibrations caused by the motors. The circular pattern is difficult to perform. It is more orthogonal than circular.

The robot can easily cover most of the 8.5" by 11" sheet of paper. However, when moving the pen closer to the

base, the pen stops touching the paper. The workspace limits do perform as presented.

4.2 Analysis and possible improvements

With the results acquired, there are certain points that can be improved.

4.2.1 Line quality

For the line quality, the problem can be divided into two solutions. The first solution is a better PWM management to smooth out the change of direction and the increase of the motor's speed. At slightly higher speed, the behavior of the motors would be more stable and more torque could be had. This can be achieved via the addition of a printed gearbox with a preferable ratio of 1:5 and with the least amount of backlash possible. The microstepping could be lowered at that moment. The second solution is the resolution of the input. With an higher Analog-Digital Converter (ADC) register size, such as the µcontroller stm32 Nucleo-64 with a 16-bit register compared to the Atmel AtMega2560 with a 10-bit register, the modulation of the speed would be more precise. Furthermore, joysticks with a greater electrical angular range could help the user to vary the input speed more easily and gradually.

4.2.2 Sagging

To ensure the biggest workspace with the robot's configuration, the pen's plan of motion must be parallel to the sheet of paper. However, there is possible play in the joints. Its effect, presented in Figure 11 (a), is the sagging of the distal bars. When this sagging is present, the pen is not orthogonal to the sheet of paper, presented in the figure Figure 11 (b). Therefore, the workspace is greatly reduced. Iterative testing of the printed arms is necessary to find and achieve sufficient tolerance to reduce play while keeping the friction to a minimum.

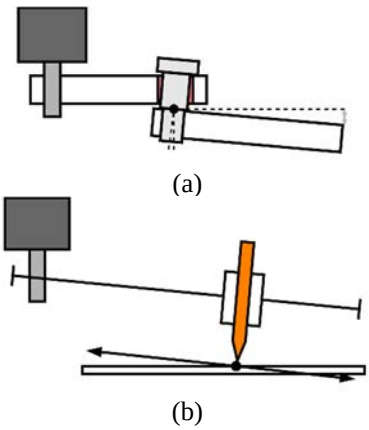

(a) (b)

Figure 11 Play in the shoudler screw's bore causing sag in the robot (a) and the effect of sag on the pen holder's horizontal alignment

5 Conclusion

This project had the objective of developing a low-cost robot able to move a pen with the direct control of its user via a controller. In this scope, the first prototype proved promising in achieving these goals. The future of this projects will primarily consist of testing with physical medicine and rehabilitation (PM&R) professionals. Following their results and feedback, the system will be improved by the laboratory's team. Moreover, some technical improvements could be done, such as the writing quality, the reduction of the overall system footprint and the optimisation of the components for a reduction of the system's cost. There is needed testing to be done for the implementation of these improvements. It is considered to upgrade the controller and change the motor drivers. Moreover, an added gearbox custom made from 3D printed part could be tested to increase the motion. Overall, there will be subsequent versions of the robotic assistant, following the evaluations from medical professionnals. In conclusion, this project has the capability to provide an affordable assistance in handwriting and clinical studies. There is potential foor this system to be used for other purposes, such as maneuvering a maze or a small parkour.

Acknowledgement
This work is supported by the Natural Sciences and Engineering Research Council of Canada (NSERC).

References

[1] American Psychiatric Association, *Developmental Coordination Disorder (F82),* In: *"Neurodevelopmental Disorders," Diagnostic and Statistical Manual of Mental Disorders*, Vol. 5, No. 5, 2022. https://doi.org/10.1176/appi.books.9780890425787.x01_neurodevelopmental_disorders

[2] ZWICKER, J.G, MISSIUNA, C., BOYD, L.A.: Neural Correlates of Developmental Coordination Disorder: A Review of Hypotheses, *Journal of Child Neurology*, Vol. 24, No. 10, pp. 1273-1281, 2009. https://doi.org/10.1177/0883073809333537

[3] MISSIUNA, C., RIVARD, L., POLLOCK, N.: They're Bright but Can't Write: Developmental Coordination Disorder in school aged children, *TEACHING Exceptional Children Plus*, Vol. 1, No. 1, pp. 1-11, 2004.

[4] HANDS, B., LARKIN, D.: *Physical Fitness and Developmental Coordination Disorder*, In: CERMAK, S.A., LARKIN, D. (ed.) *Developmental Coordination Disorder*, Albany, DELMAR, pp. 172-176, 2002.

[5] CASE-SMITH, J., WEINTRAUB, N.: *Hand function and Developmental Coordination Disorder,* In: CERMAK, S.A., LARKIN, D. (ed.) *Developmental Coordination Disorder*, Albany, DELMAR, pp. 163-171, 2002.

[6] SMOKER, T.J., MURPHY, C.E., ROCKWELL, A.K.: Comparing Memory for Handwriting versus Typing,

Proceedings of the Human Factors and Ergonomics Society Annual Meeting, Vol. 53, No. 22, pp. 1744-1747, 2009. https://doi.org/10.1177/154193120905302218

[7] KLASS, P.: Why Handwriting Is Still Essential in the Keyboard Age, Well, [Online], Available: https://archive.nytimes.com/well.blogs.nytimes.com/2016/06/20/why-handwriting-is-still-essential-in-the-keyboard-age [10 Jun 2024], 2016.

[8] MUELLE, P.A., OPPENHEIMER, D.M.: The Pen is Mightier Than the Keyboard: Advantages of Longhand Over Laptop Note Taking, *Psychological Science*, Vol. 25, No. 6, pp. 1159-1168, 2014. https://doi.org/10.1177/0956797614524581

[9] Writing Bird, Healthcare Solutions, [Online], Available: https://healthcaresolutions.ca/products/writing-bird [10 Jun 2024], 2024.

[10] Wanchick's Writer 2 - Discontinued, ArthritisSupplies.com, [Online], Available: https://www.arthritissupplies.com/wanchiks-writer-2.html [10 Jun 2024], 2024.

[11] LEMIRE, G.: *Aide à l'écriture pour les enfants vivant aves des incoordinations de mouvement*, M.S. Thesis, Laval University, Quebec City, 2020. (Original in French)

[12] SHIRE, K.A., HILL, L.J.B., SNAPP-CHILDS, W., BINGHAM, G.P., KOUNTOURIOTIS, G.K., BARBER, S., MON-WILLIAMS, M.: Robot Guided 'Pen Skill' Training in Children with Motor Difficulties, *PLOS ONE*, Vol. 11, No. 3, pp. 1-14, 2016. https://doi.org/10.1371/journal.pone.0151354

[13] Phantom Omni – 6 DOF master device, Delft Haptics Lab, [Online], Available: https://delfthapticslab.nl/device/phantom-omni [10 Jun 2024], 2024.

[14] Geomagic Touch Haptic Device, GoMeasure3D, [Online], Available: https://shop.gomeasure3d.com/products/geomagic-touch-haptic-device [10 Jun 2024], 2024.

[15] AxiDraw SE/A3, Evil Mad Scientist, [Online], Available: https://shop.evilmadscientist.com/productsmenu/908 [10 Jun 2024], 2024.

[16] AxiDraw SE/A3 Personal Writing & Drawing Robot (Intl), RobotShop Europe, [Online], Available: https://eu.robotshop.com/products/axidraw-se-a3-personal-writing-drawing-robot-intl [10 Jun 2024], 2024.

Review process
Single-blind peer review process.

JOURNAL STATEMENT

Journal name:	**Acta Tecnología**
Abbreviated key title:	Acta Tecnol
Journal title initials:	AT
Journal doi:	10.22306/atec
ISSN:	2453-675X
Start year:	2015
The first publishing:	October 2015
Issue publishing:	Quarterly
Publishing form:	On-line electronic publishing
Availability of articles:	Open Access Journal
Journal license:	CC BY-NC
Publication ethics:	COPE, ELSEVIER Publishing Ethics
Plagiarism check:	Worldwide originality control system
Peer review process:	Single-blind review at least two reviewers
Language:	English
Journal e-mail:	**info@actatecnologia.eu**

The journal focuses mainly on the original and new, interesting, high-quality, theoretical, practical and application-oriented contributions to science and research and pedagogy and education in technologies.

Acta Tecnologia journal supports the San Francisco Declaration on Research Assessment (DORA). The primary directives include open access, reuse of outputs, diversity among authors and reviewers, peer review, description of provided services and related publishing charges.

Publisher:	**4S go, s.r.o.**
Address:	Semsa 24, 044 21 Semsa, Slovak Republic, EU
Phone:	+421 948 366 110
Publisher e-mail:	**info@4sgo.eu**

Responsibility for the content of a manuscript rests upon the authors and not upon the editors or the publisher.